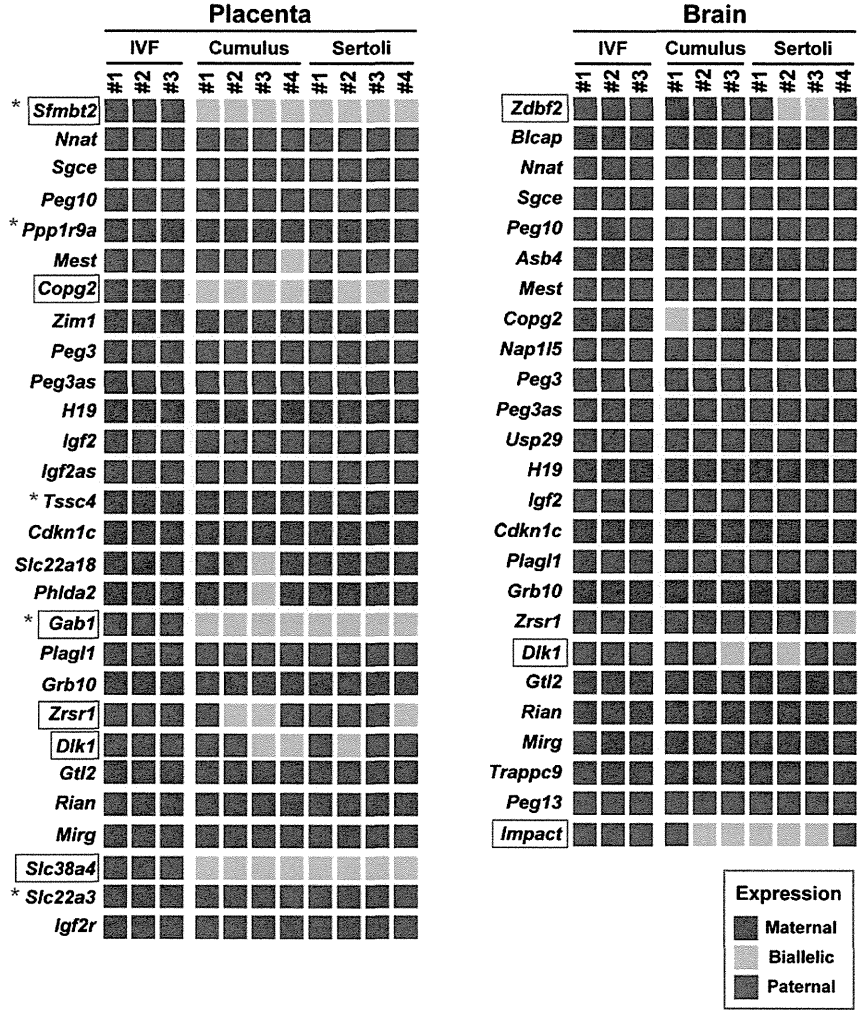

Figure 1. Transcriptome-wide analyses of imprinted gene expression in cloned mouse placentas and brains. The maternal read number divided by the paternal read number (M/P ratio) is color-coded. The maternal expression (red) and paternal expression (blue) are defined as [M/P ratio] >2 and [M/P ratio] <0.5, respectively. The biallelic expression (green) is defined as $2 \geq$ [M/P ratio] ≥ 0.5. Imprinted genes that showed abnormal allelic expression in at least two cloned placentas or brains are indicated by red boxes. Placenta-specific imprinted genes are marked with asterisks.

derived from cumulus clones #3 and #4 and Sertoli clone #2 (Fig. 4B and Supplementary Material, Fig. S4A). In the brains derived from cumulus clone #3 and Sertoli clone #2, *Dlk1* also showed biallelic expression (Fig. 4B). In the cloned mouse brains, biallelic expression of *Dlk1* correlated with increased expression of *Dlk1* (Fig. 4C). In the brains derived from cumulus clone #3 and Sertoli clone #2, biallelic expression of *Begain* and *Rtl1* (Supplementary Material, Fig. S4B) and downregulation of *Gtl2*, *Rian* and *Mirg* (Fig. 4C) were observed. Abnormal allelic expression of *Gtl2* was not observed in the cloned mouse brains (Supplementary Material, Fig. S4B).

In the cloned mouse placentas, the expression level of genes in the *Dlk1-Dio3* domain was extremely low regardless of allelic expression of *Dlk1* (Supplementary Material, Fig. S4C). In the placenta, *Dlk1* and *Gtl2* are mainly expressed in the labyrinth layer (25,26). The junctional zone, where *Dlk1* and *Gtl2* are not (or weakly) expressed, is expanded in the cloned mouse placenta (25). Therefore, low expression of *Dlk1* and *Gtl2* may, in part, be explained by the expansion of the junctional zone (relative reduction of the labyrinth layer) in the cloned mouse placenta.

Imprinting of the *Dlk1-Dio3* domain is regulated by the IG-DMR (24). Paternal methylation of the IG-DMR was observed in both the donor cells and the IVF-derived brain (Supplementary Material, Fig. S4D), but in the brains derived from cumulus clone #3 and Sertoli clone #2, both alleles were methylated (Fig. 4D). In the whole fetus of cumulus clone #4, gain of maternal methylation of the IG-DMR was also observed (Fig. 4D). Gain of maternal methylation of the IG-DMR was also found in the cloned placentas (Supplementary Material, Fig. S4E). Similar data were obtained for the *Gtl2*-DMR (Supplementary Material, Fig. S5).

Placental development without a viable fetus is frequently observed in SCNT (27). We compared the imprinting status of the *Dlk1-Dio3* domain in term placentas with and without viable fetuses, which were produced by a series of experiments using *Xist*-siRNA (Supplementary Material, Table S2). The use

Downloaded from http://hmg.oxfordjournals.org/ at Tohoku University on March 1, 2014

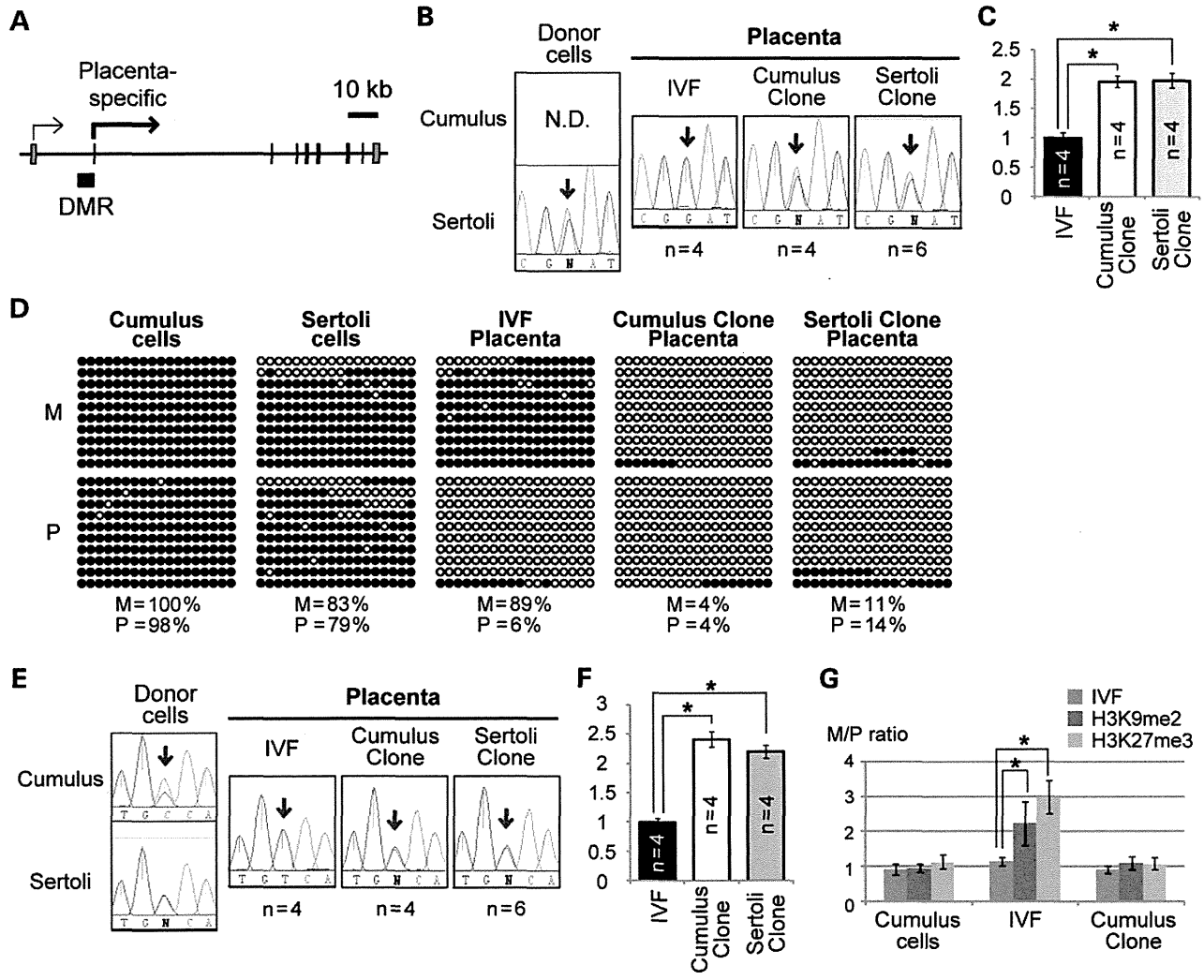

Figure 2. Consistent loss of *Gab1* and *Sfmbt2* imprinting in cloned mouse placentas. (**A**) Genomic structure of *Gab1*. The *Gab1* DMR and two transcription start sites are shown. Expression from the placenta-specific promoter was analyzed in this study. (**B**) Allelic expression of *Gab1*. *Gab1* showed paternal expression in all IVF-derived placentas but showed biallelic expression in all cloned mouse placentas. The numbers of analyzed samples are shown. Very similar data were obtained for all cloned placentas. The SNP site between 129 and JF1 is indicated by arrows. N.D.: not detected. (**C**) Real-time RT–PCR analysis of *Gab1*. The mean expression level of the IVF-derived placentas is set as 1. The error bars indicate means ± SD of four placentas. $^*P < 0.001$ (Student's *t*-test). (**D**) DNA methylation analysis of the *Gab1* DMR by bisulfite sequencing. Black and white circles indicate methylated and unmethylated residues, respectively. The percentages of methylated CpG sites of the maternal allele (M) and the paternal allele (P) are indicated. (**E**) Allelic expression of *Sfmbt2*. *Sfmbt2* showed paternal expression in all IVF-derived placentas but showed biallelic expression in all cloned mouse placentas. The numbers of analyzed samples are shown. Very similar data were obtained for all cloned placentas. (**F**) Real-time RT–PCR analysis of *Sfmbt2*. The error bars indicate means ± SD of four placentas. $^*P < 0.001$ (Student's *t*-test). (**G**) Histone modifications at *Sfmbt2* promoter region by chromatin immunoprecipitation (ChIP) and single nucleotide primer extension (SNuPE). The amount of immunoprecipitated DNA derived from the maternal allele is divided by that from the paternal allele (M/P ratio). The error bars indicate means ± SD from three samples. $^*P < 0.05$ (Student's *t*-test).

of *Xist*-siRNA increases cloning efficiency (18) and enables the comparison of placentas with and without viable fetuses within the same experiment. Biallelic expression of *Dlk1* was consistently observed in placentas, brains and fetuses (Fig. 4B and Supplementary Material, Fig. S4A). Therefore, if *Dlk1* shows biallelic expression in the placenta, it is predicted that *Dlk1* would also show biallelic expression in the brain and fetus. A clear increase of abnormal maternal expression of *Dlk1* was observed in the placentas without viable fetuses compared with the placentas with viable fetuses ($P < 10^{-9}$) (Fig. 4E), alongside hypermethylation of the IG-DMR (Supplementary Material, Fig. S6). On the other hand, allelic expression profiles of *Sgce* and *Zim1* were comparable between placentas with viable fetuses and without viable fetuses ($P > 0.05$, Supplementary Material, Fig. S4F).

Confirmation of loss of imprinting in cloned mouse placentas produced without trichostatin A (TSA) treatment

Figures 1–4 present data from cloned mouse embryos produced using TSA to increase cloning efficiency. TSA treatment might affect allelic expression of some imprinted genes. Therefore, we confirmed biallelic expression of *Gab1*, *Sfmbt2* and *Slc38a4* in four cloned mouse placentas produced without TSA treatment (Supplementary Material, Fig. S3B). Similarly, biallelic

Downloaded from http://hmg.oxfordjournals.org/ at Tohoku University on March 1, 2014

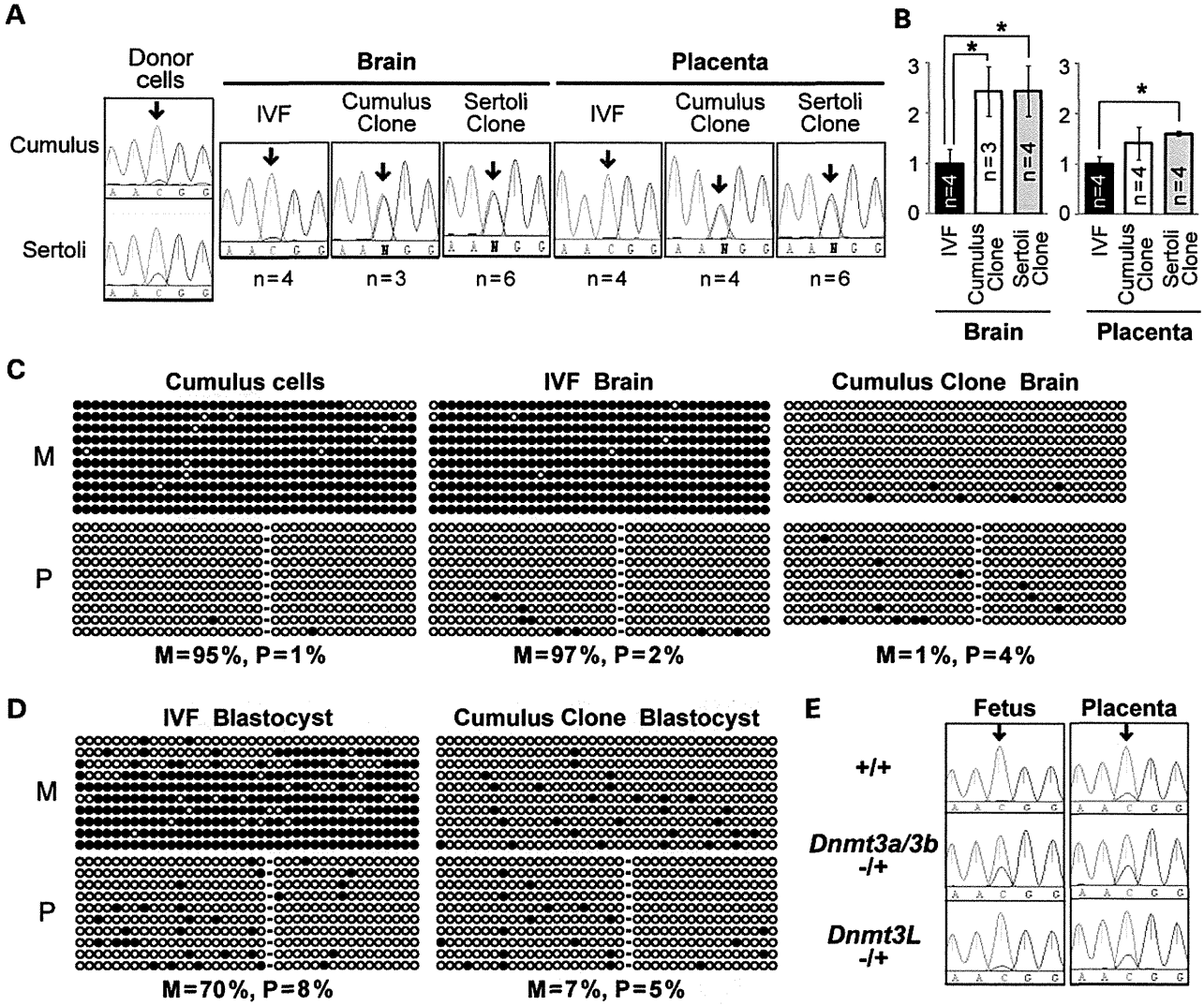

Figure 3. Consistent loss of *Slc38a4* imprinting in cloned mice. (**A**) Allelic expression of *Slc38a4*. *Slc38a4* showed paternal expression in IVF-derived samples but showed biallelic expression in all cloned mouse brains and placentas analyzed. The numbers of analyzed samples are shown. Very similar data were obtained for all cloned samples. (**B**) Real-time RT–PCR analysis of *Slc38a4*. The mean expression level of the IVF-derived samples is set as 1. The error bars indicate means ± SD of three or four samples. $^*P < 0.05$ (Student's *t*-test). (**C**) DNA methylation analysis of the *Slc38a4* DMR in cumulus cells and brains. Black and white circles indicate methylated and unmethylated residues. The percentages of methylated CpG sites of the maternal allele (M) and the paternal allele (P) are indicated. (**D**) DNA methylation analysis of the *Slc38a4* DMR in cloned blastocysts. (**E**) Allelic expression of *Slc38a4* in the concepti obtained from *Dnmt3L*-deficient and oocyte-specific *Dnmt3a/3b*-deficient females.

expression of *Dlk1* was observed in two of four cloned mouse placentas produced without TSA treatment (Supplementary Material, Fig. S4G). These data indicated that loss of *Gab1*, *Sfmbt2*, *Slc38a4* and *Dlk1* imprinting was caused by SCNT, not by TSA treatment.

Characteristics of genes with consistent loss of imprinting in cloned mice

As described earlier, *Gab1*, *Sfmbt2* and *Slc38a4* showed consistent loss of imprinting in cloned mice. These three genes were all maternally repressed and did not require *de novo* DNA methylation in growing oocytes for the establishment of imprinting (Table 1). No paternally methylated germline DMR has been found near these genes in the recent whole-genome DNA methylation analysis of germ cells (23). Importantly, these genes showed normal expression levels in the placentas of bi-maternal embryos that contained genomes from non-growing and fully grown oocytes (Table 1 and (28)). If a paternally expressed gene is not regulated by maternal imprinting, it is repressed in bi-maternal embryos (Supplementary Material, Fig. S7A). For example, *Igf2* and *Dlk1*, which are paternally expressed and regulated by paternal imprinting, showed greatly reduced expression in bi-maternal embryos compared with wild-type embryos (Table 1). These data suggest that imprinting of *Gab1*, *Sfmbt2* and *Slc38a4* may be

Downloaded from http://hmg.oxfordjournals.org/ at Tohoku University on March 1, 2014

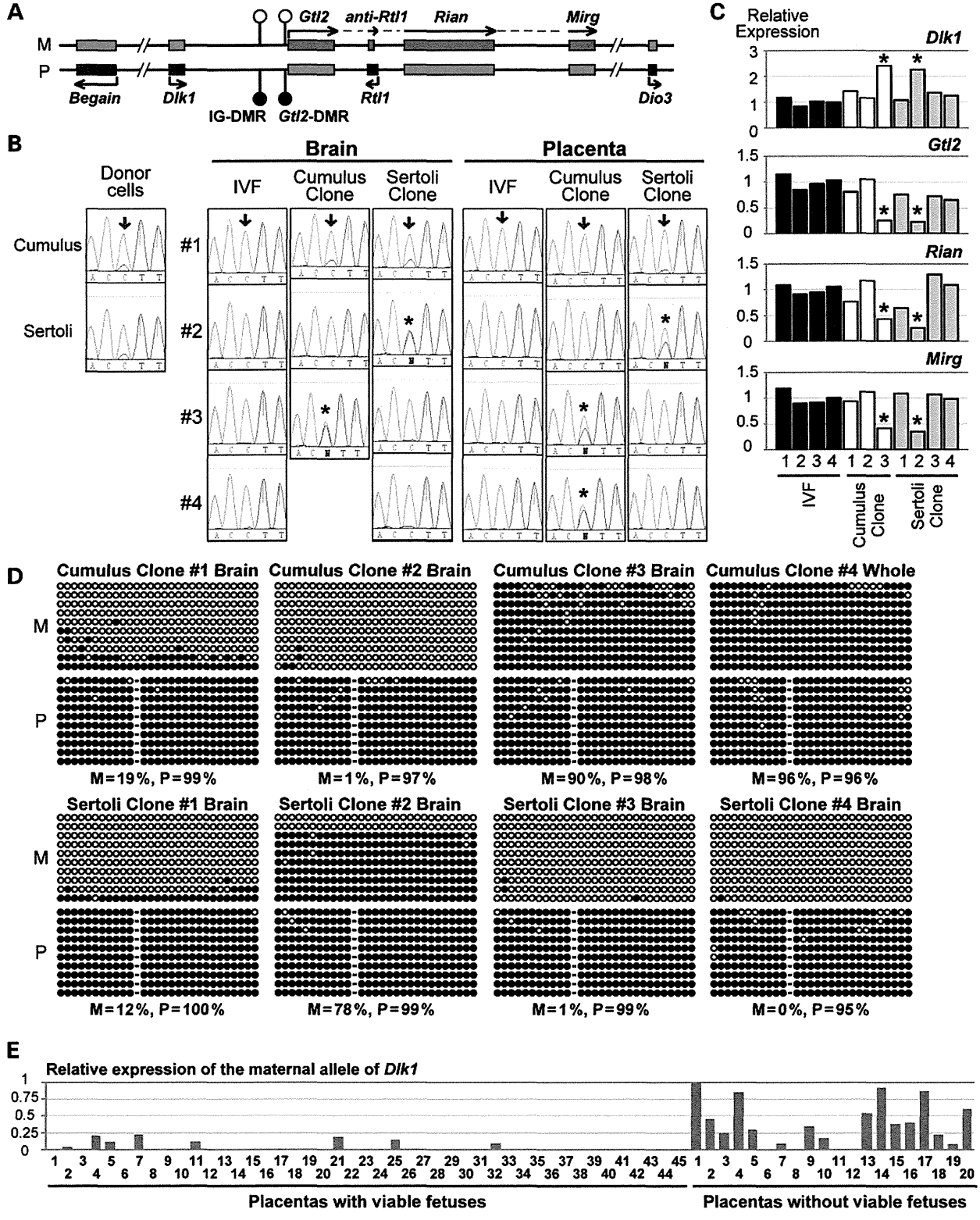

Figure 4. Loss of *Dlk1-Dio3* imprinting and embryonic lethality in cloned mice. (**A**) Genomic structure of the *Dlk1-Dio3* domain. Maternally expressed genes and paternally expressed genes are in red and blue, respectively. Open circles and filled circles indicate unmethylated and methylated DMRs, respectively. M, maternal allele; P, paternal allele. (**B**) Allelic expression of *Dlk1*. Biallelic expression is marked with an asterisk. For cumulus clone #4, the brain sample was not analyzed because of severe growth retardation of this clone. (**C**) Real-time RT–PCR analysis of *Dlk1*, *Gtl2*, *Rian* and *Mirg* in the brain. The mean expression level of the

Downloaded from http://hmg.oxfordjournals.org/ at Tohoku University on March 1, 2014

Table 1. Unique characteristics of Gab1, Sfmbt2 and Slc38a4

Gene	Frequency of loss of imprinted expression	*de novo* DNA methylation in growing oocytes	Expression in bi-maternal placentas (fold decrease)
Gab1	14/14[a]	Not required(19)	1.38 ± 0.12
Sfmbt2	14/14[a]	Not required(19)	1.31 ± 0.39
Slc38a4	14/14[a]	Not required	1.07 ± 0.15
Igf2	0/8	Not required[$b]	37.9 ± 14.8[c]
Dlk1	5/12	Not required[$b]	24.5 ± 5.4[c]
Peg10	0/8	Required[$b]	1.03 ± 0.22
Mest	1/8	Required[$b]	1.38 ± 0.47
Peg3	0/8	Required[$b]	1.13 ± 0.15

Paternally expressed genes known to be regulated by DNA methylation during spermatogenesis (*Igf2* and *Dlk1*) and oogenesis (*Peg10*, *Mest* and *Peg3*) are included for comparison. The frequency of loss of imprinted expression is based on results obtained using E13.5 cloned mouse placentas. Microarray data of bi-maternal placentas (28) are used for the calculation of the fold decrease (means ± SD from three replicates).
[a]Statistically significant compared with IVF embryos ($P < 0.05$, Fisher's exact test).
[$b]See Supplementary Material, Figure S7B.
[c]Statistically significant compared with control placentas ($P < 0.05$, Student's *t*-test).

established during oocyte growth in a *de novo* DNA methylation-independent manner.

DISCUSSION

Relationships between developmental abnormalities and imprinting defects in cloned mice

We found a correlation between embryonic lethality and loss of *Dlk1-Dio3* imprinting. Loss of *Dlk1-Dio3* imprinting in cloned mice was caused by the paternalization of the maternal allele, which is very similar to the maternal transmission of IG-DMR knockout allele (ΔIG-DMR/+). While ΔIG-DMR/+ fetuses are perinatal lethal and show muscle and skeletal defects at late gestational stage, the overall growth performance is normal (24). On the other hand, cloned fetuses with loss of *Dlk1-Dio3* imprinting were absorbed by term, and muscle and skeletal defects at late gestational stage thus cannot be analyzed. While the underlying mechanism of the fetal absorption is unclear, these data suggest that the combination of loss of *Dlk1-Dio3* imprinting and other abnormalities may cause earlier embryonic death in cloned mice. Loss of *Dlk1-Dio3* imprinting is also observed in various induced pluripotent stem cell (iPSC) lines (29), highlighting the similarity of two reprograming strategies, SCNT and iPSC production. It has not yet been determined why loss of *Dlk1-Dio3* imprinting occurs in cloned mice and iPSCs. However, it is reported that high expression of Oct4 and Klf4 combined with lower expression of c-Myc and Sox2 prevents loss of *Dlk1-Dio3* imprinting in iPSCs (30). Cloned mouse embryos frequently show reduced or ectopic expression of Oct4 during the preimplantation stage (31), and it is possible that abnormal expression of Oct4 induces loss of *Dlk1-Dio3* imprinting in cloned mice.

Placentomegaly is observed in all cloned mouse concepti (3). *Sfmbt2* is the only known protein-coding gene in proximal chromosome 2. The paternal duplication of proximal chromosome 2, which causes overexpression of *Sfmbt2*, is known to result in placentomegaly (32). In contrast, deficiency of *Gab1* is known to result in the reduction of placental size (33). The overexpression of *Sfmbt2* and *Gab1* observed in cloned placentas might be involved in placentomegaly of cloned mice. It is also proposed that imprinted expression of *Slc38a4* in the placenta may be important for the normal supply of neutral amino acids to the fetus (34). Thus *Slc38a4*-knockout or -transgenic mice, which have not been reported, merit further investigation to understand the phenotypic abnormalities of cloned animals.

While we focused on imprinted genes in this study, many non-imprinted genes were also reported to show aberrant expression in cloned mice, especially in the placenta (35). Aberrant expression of both imprinted genes and non-imprinted genes may impact the size and viability of cloned mouse embryos.

Consistent loss of imprinting caused by incomplete imprinting memory in somatic cells

Two placenta-specific imprinted genes, *Gab1* and *Sfmbt2*, showed complete loss of imprinting in all cloned placentas analyzed. In the donor cells, neither gene showed imprinted expression. In the promoter region, allele-specific DNA methylation of *Gab1* and allelic enrichment of histone modifications of *Sfmbt2* were not observed in donor cells or cloned placentas. These data suggested that the imprinting of *Gab1* and *Sfmbt2* was not retained in somatic cells and not reinstated in the placental lineages derived from cloned somatic cells.

In addition to *Gab1* and *Sfmbt2*, there are several additional genes that show tissue-specific imprinted expression. We found that four placenta-specific and three brain-specific imprinted genes showed normal monoallelic expression in the cloned mice. These seven genes are all present within imprinted gene clusters that have germline DMRs, but *Gab1* and *Sfmbt2* are not. It is likely that monoallelic expression of these seven tissue-specific imprinted genes was reestablished after SCNT, using imprinting marks retained in the clusters.

Slc38a4 shows imprinted expression both in the normal fetus and placenta (22), and imprinted methylation at the *Slc38a4* DMR was maintained in the donor cells. However, the *Slc38a4* DMR of somatic cells was not protected from demethylation during preimplantation development. Interestingly, paternal expression of *Slc38a4* was not lost in embryos obtained from *Dnmt3L*-deficient and oocyte-specific *Dnmt3a/3b*-deficient female mice. Therefore, we hypothesize that, during oogenesis,

IVF-derived samples is set as 1. Samples with biallelic expression of *Dlk1* are marked with an asterisk. (**D**) DNA methylation analysis of the IG-DMR by bisulfite sequencing in cloned mouse brains. The DNA methylation of cumulus clone #4 was analyzed in the whole fetus. The percentages of methylated CpG sites are indicated. (**E**) Summary of allelic expression of *Dlk1* in term placentas from a series of experiments using *Xist*-siRNA (see Supplementary Material, Table S2 for details). Donor cells were collected from [B6xDBA]F1 mice. The expression level of the maternal allele of *Dlk1* is normalized by that of the paternal allele. Forty-five placentas with viable fetuses and 20 placentas without viable fetuses (the fetus of #11 was small and dead, and the other fetuses were absorbed) were analyzed. Increased expression of the maternal allele of *Dlk1* is observed in the placentas without viable fetuses ($P < 10^{-9}$, Student's *t*-test).

Downloaded from http://hmg.oxfordjournals.org/ at Tohoku University on March 1, 2014

Slc38a4 acquires an imprinting mark[s] other than DNA methylation, which is required for the protection of the *Slc38a4* DMR from demethylation during preimplantation development but which is lost in somatic cells.

Gab1, *Sfmbt2* and *Slc38a4* may not require *de novo* DNA methylation for the establishment of imprinting (Table 1). *De novo* DNA methylation has already been shown to be dispensable for imprinting of the maternal X-chromosome (36), and *Xist* shows ectopic expression in nearly all cloned mouse embryos (16). It is interesting to speculate that the *de novo* DNA methylation-independent establishment of imprinting may be a common feature of imprinted genes showing consistent imprinting defects in cloned mice.

In conclusion, we found that *Gab1*, *Sfmbt2* and *Slc38a4* showed consistent loss of imprinting in cloned mice. It is likely that an imprinting mark[s] other than DNA methylation may be required for the establishment of imprinting of these genes. We also verified the correlation between loss of *Dlk1-Dio3* imprinting and embryonic lethality of cloned mice. These findings will have value both for elucidating the mechanisms involved in reprograming and also determining the potential risks of clinical applications of nuclear reprograming.

MATERIALS AND METHODS

Ethics statement

All animal experiments were performed at RIKEN Tsukuba Institute in accordance with the Animal Experimentation Committee's guiding principles.

SCNT

To generate [129xJF1]F1 mice, 129 females were mated with JF1 males. B6 females were mated with DBA males to generate [B6xDBA]F1 mice. Nuclear transfer was carried out with a Piezo-driven micromanipulator (PMM-150FU, Prime Tech, Ibaraki, Japan) as described in Wakayama *et al.* (37) and Ogura *et al.* (38). For the preparation of nuclear donor cells, cumulus cells were collected from female mice at 8–12 weeks of age, and Sertoli cells were collected from male mice at 1–9 days of age as described in Ogura *et al.* (38). Donor nuclei were injected into enucleated recipient oocytes collected from [B6xDBA]F1 female mice, and the reconstructed embryos were treated with 50 nM TSA (Sigma–Aldrich, St. Louis, MO, USA) for 8 h in total. To obtain the data shown in Supplementary Material, Figures S3B and S4G, the reconstructed embryos were not treated with TSA. For the analyses of term placentas, microinjection of *Xist*-siRNA was performed as described in Matoba *et al.* (18). After nuclear transfer, some embryos in the two-cell stage were transferred to pseudopregnant ICR mice, and others were collected at the blastocyst stage. [129xJF1]F1 embryos generated by conventional IVF (39) were used as controls for allelic expression and epigenetic analyses. Cloned embryos were delivered by cesarean section, and only placentas were collected and used for the analyses, shown in Figure 4E and Supplementary Material, Figure S4F. In the case that neonates at birth were alive, placentas were classified as 'placentas with viable fetuses'. In the case that fetuses were dead or absorbed, placentas were classified as 'placentas without viable fetuses'.

Whole transcriptome sequencing and data analysis

Total RNA was extracted from brains and placentas of E13.5 embryos. Four micrograms of total RNA was used for library construction using TruSeq RNA Sample Prep Kit v2 (Illumina, CA, USA) according to the manufacturer's protocol. Briefly, poly-A-containing mRNAs were purified using poly-T oligo-attached magnetic beads. The purified mRNAs were fragmented using divalent cations under elevated temperatures and then converted to dsDNA by two rounds of cDNA synthesis using reverse transcriptase and DNA polymerase I. After an end repair process, DNA fragments were ligated with adaptor oligos. The ligated products were amplified using 15 cycles of PCR to generate an RNA-seq library. Library integrity was verified by Bioanalyzer DNA1000 assay (Agilent Technologies, CA, USA). Sequencing was performed in 39-bp paired-end mode using a Genome Analyzer IIx (Illumina).

A total of 2 012365 798 reads were obtained for 25 samples. Sequenced reads were all filtered by the sequence quality score. If the average quality score of at least one of a paired read was <20, the paired read was discarded. Filtered reads were mapped to the reference mouse genome (UCSC mm9) by using Novoalign (V.2.07.13) (http://novocraft.com/) with the parameter '-r Random'. Mapping results were further processed using the Picard MarkDuplicate program (version 1.67) (http://picard.sourceforge.net/) to remove duplicate reads. Samples obtained from 129 and JF1 inbred mice were used for the identification of SNPs. SNP candidates were searched for with the The Genome Analysis Toolkit (GATK) (version 1.6–5) (40) according to its recommended procedure, and a total of 1 756 512 SNPs were identified. SNPs meeting the following criteria were used for further analysis: $\geq 90\%$ reads of 129-derived samples and $<10\%$ reads of JF1-derived samples identical to the reference sequence, or the opposite case.

Known imprinted genes were selected based on imprinted gene databases (http://igc.otago.ac.nz/ and http://www.har.mrc.ac.uk/). Imprinted genes annotated by RefSeq, except miRNAs and snoRNAs, were analyzed. Placenta-specific imprinted genes *Tfpi2*, *Tspan32*, *Cd81* and *Ano1* were excluded because these genes were highly expressed by maternal cells in the placenta. Only genes that had at least one SNP site with ≥ 10 reads in all brain or placental samples were used for the allelic expression analysis. For the analyses of allelic expression of imprinted genes, we used all mapped reads for all SNPs identified (including SNPs with <10 reads), and the numbers of paternal and maternal reads were summed for each gene. The maternal read number divided by the paternal read number (M/P ratio) was calculated. The maternal expression and paternal expression are defined as [M/P ratio] >2 and [M/P ratio] <0.5, respectively.

Preparation of embryos from *Dnmt3L*-deficient and oocyte-specific *Dnmt3a/3b*-deficient females

Production of mice with the conditional alleles, referred to as $Dnmt3a^{2lox}$ and $Dnmt3b^{2lox}$, was described previously (5,41). To disrupt the conditional alleles in growing oocytes, the mice were crossed with those carrying a *Zp3*-Cre gene (42). The precise timing of conditional deletion of *Dnmt3a* and *Dnmt3b* by *Zp3*-Cre is described elsewhere (43). By crossing [$Dnmt3a^{2lox/2lox}$, $Dnmt3b^{2lox/2lox}$, *Zp3*-Cre] females with wild-type

Downloaded from http://hmg.oxfordjournals.org/ at Tohoku University on March 1, 2014

JF1 male mice, we obtained [*Dnmt3a*$^{-/+}$, *Dnmt3b*$^{-/+}$] E9.5 embryos. *Dnmt3L*-knockout female mice (44) were also crossed with wild-type JF1 male mice to obtain *Dnmt3L*$^{-/+}$ E9.5 embryos.

Real-time RT–PCR

Total RNA was prepared using an RNeasy mini Kit and RNase-free DNase (Qiagen, CA, USA). First-strand cDNA was synthesized from total RNA using PrimeScript II (Takara Bio, Shiga, Japan). Real-time PCR reaction was done with SYBR Premix Ex Taq II (Takara Bio). The amount of target mRNA was determined from the appropriate standard curve and normalized to the amount of *β-actin* mRNA. The primer sets are shown in Supplementary Material, Table S3.

Analysis of allelic expression

PCR amplification was performed using KOD FX (TOYOBO, Osaka, Japan). PCR products were Sanger-sequenced, and the sequence chromatograms were analyzed with Sequencing Analysis Software v5.4 (Applied Biosystems, CA, USA). Multiple sequence alignments were done using GENETYX version 10.0.3 (GENETYX, Tokyo, Japan). For the quantification of expression alleles in Figure 4E, the peak heights of sequence chromatograms were used as expression levels. The allelic expression of *Rtl1* was analyzed using 3′ rapid amplification of cDNA ends (RACE) as previously reported (45). The primer sets and SNP positions are shown in Supplementary Material, Table S3.

Bisulfite sequencing

DNA samples were treated with sodium bisulfite using an EZ DNA Methylation Kit (Zymo Research, Orange, CA) and PCR-amplified using TaKaRa EpiTaq^{TM} HS (Takara Bio). The PCR products were cloned into the pGEM-T Easy vector (Promega, Wisconsin, USA), and individual clones were sequenced. Primers used are listed in Supplementary Material, Table S3.

ChIP and SNuPE

ChIP analysis was performed using a Magna ChIP G Chromatin Immunoprecipitation Kit (Millipore, Temecula, CA) according to the manufacturer's protocol. The following antibodies were used: dimethylated H3-Lys9 and trimethylated H3-Lys27 (Millipore). The precipitated DNA was PCR-amplified, and the allelic histone modifications were analyzed using SNuPE. SNuPE analysis was performed using a SNaPshot Multiplex Kit (Applied Biosystems) according to the manufacturer's protocol. The peak height was determined using GeneMapper v4.1 (Applied Biosystems). Primers used are listed in Supplementary Material, Table S3.

Imprinted gene expression in bi-maternal placentas

Microarray data for three types of bi-maternal placentas (28) were used for the expression analysis presented in Table 1. For *Dlk1*, we used the data for embryos in which the *Igf2-H19* domain in the distal region on chromosome 7 was switched from the maternal to the paternal epigenotype. For *Igf2*, we used the data for embryos in which the *Dlk1-Dio3* domain in the distal region on chromosome 12 was switched from the maternal to the paternal epigenotype. For other imprinted genes, we used the data for embryos in which the both domains in the distal regions on chromosomes 7 and 12 were switched from the maternal to the paternal epigenotype.

5′ RACE

5′ RACE analysis of *Gab1* was performed using a CapFishing Full-length cDNA Isolation Kit (Seegene, Maryland, USA). The gene specific-primer sequence was 5′-GACTGGAGGCTGGTGCT GTACTTA-3′.

Accession numbers

All sequencing data are deposited in DDBJ Sequence Read Archive (DRA) under the accession number DRA000627.

SUPPLEMENTARY MATERIAL

Supplementary Material is available at *HMG* online.

ACKNOWLEDGEMENTS

We thank Ms N. Miyauchi, Ms F. Sato, Ms M. Tsuda, Ms N. Koshita, Ms M. Kikuchi and Mr K. Kuroda for technical assistance and Dr Rosalind M. John for support and valuable suggestions. The microarray data of bi-maternal placentas were kindly provided by Dr T. Kono and Mr F. Cao. We also thank the Biomedical Research Core of Tohoku University Graduate School of Medicine for technical support.

Conflict of Interest statement. None declared.

FUNDING

This work was supported by Grants-in-Aid for Scientific Research (KAKENHI) from Japan Society for the Promotion of Science (22800084, 23220011, 23390385, 24613001 and 25670691), KAKENHI from the Ministry of Education, Culture, Sports, Science and Technology (20062010, 23013003 and 25112009) and the Takeda Science Foundation.

REFERENCES

1. Dean, W., Santos, F. and Reik, W. (2003) Epigenetic reprogramming in early mammalian development and following somatic nuclear transfer. *Semin. Cell Dev. Biol.*, **14**, 93–100.
2. Jouneau, A. and Renard, J.P. (2003) Reprogramming in nuclear transfer. *Curr. Opin. Genet. Dev.*, **13**, 486–491.
3. Yang, X., Smith, S.L., Tian, X.C., Lewin, H.A., Renard, J.P. and Wakayama, T. (2007) Nuclear reprogramming of cloned embryos and its implications for therapeutic cloning. *Nat. Genet.*, **39**, 295–302.
4. Surani, M.A. (1998) Imprinting and the initiation of gene silencing in the germ line. *Cell*, **93**, 309–312.
5. Kaneda, M., Okano, M., Hata, K., Sado, T., Tsujimoto, N., Li, E. and Sasaki, H. (2004) Essential role for de novo DNA methyltransferase Dnmt3a in paternal and maternal imprinting. *Nature*, **429**, 900–903.

Downloaded from http://hmg.oxfordjournals.org/ at Tohoku University on March 1, 2014

6. Bourc'his, D., Xu, G.L., Lin, C.S., Bollman, B. and Bestor, T.H. (2001) Dnmt3l and the establishment of maternal genomic imprints. *Science*, **294**, 2536–2539.
7. Ferguson-Smith, A.C. (2011) Genomic imprinting: the emergence of an epigenetic paradigm. *Nat. Rev. Genet.*, **12**, 565–575.
8. Smith, F.M., Garfield, A.S. and Ward, A. (2006) Regulation of growth and metabolism by imprinted genes. *Cytogenet. Genome Res.*, **113**, 279–291.
9. Chavatte-Palmer, P., Camous, S., Jammes, H., Le Cleac'h, N., Guillomot, M. and Lee, R.S. (2012) Review: placental perturbations induce the developmental abnormalities often observed in bovine somatic cell nuclear transfer. *Placenta.*, **33**(Suppl), S99–S104.
10. Dinnyes, A., Tian, X.C. and Yang, X. (2008) Epigenetic regulation of foetal development in nuclear transfer animal models. *Reprod. Domest. Anim.*, **43**(Suppl 2), 302–309.
11. Whitworth, K.M. and Prather, R.S. (2010) Somatic cell nuclear transfer efficiency: how can it be improved through nuclear remodeling and reprogramming? *Mol. Reprod. Dev.*, **77**, 1001–1015.
12. de Waal, E., Yamazaki, Y., Ingale, P., Bartolomei, M.S., Yanagimachi, R. and McCarrey, J.R. (2012) Gonadotropin stimulation contributes to an increased incidence of epimutations in ICSI-derived mice. *Hum. Mol. Genet.*, **21**, 4460–4472.
13. Mann, M.R., Chung, Y.G., Nolen, L.D., Verona, R.I., Latham, K.E. and Bartolomei, M.S. (2003) Disruption of imprinted gene methylation and expression in cloned preimplantation stage mouse embryos. *Biol. Reprod.*, **69**, 902–914.
14. Humpherys, D., Eggan, K., Akutsu, H., Hochedlinger, K., Rideout, W.M. 3rd, Biniszkiewicz, D., Yanagimachi, R. and Jaenisch, R. (2001) Epigenetic instability in ES cells and cloned mice. *Science*, **293**, 95–97.
15. Ogawa, H., Ono, Y., Shimozawa, N., Sotomaru, Y., Katsuzawa, Y., Hiura, H., Ito, M. and Kono, T. (2003) Disruption of imprinting in cloned mouse fetuses from embryonic stem cells. *Reproduction*, **126**, 549–557.
16. Inoue, K., Kohda, T., Sugimoto, M., Sado, T., Ogonuki, N., Matoba, S., Shiura, H., Ikeda, R., Mochida, K., Fujii, T. *et al.* (2010) Impeding Xist expression from the active X chromosome improves mouse somatic cell nuclear transfer. *Science*, **330**, 496–499.
17. Inoue, K., Kohda, T., Lee, J., Ogonuki, N., Mochida, K., Noguchi, Y., Tanemura, K., Kaneko-Ishino, T., Ishino, F. and Ogura, A. (2002) Faithful expression of imprinted genes in cloned mice. *Science*, **295**, 297.
18. Matoba, S., Inoue, K., Kohda, T., Sugimoto, M., Mizutani, E., Ogonuki, N., Nakamura, T., Abe, K., Nakano, T., Ishino, F. *et al.* (2011) RNAi-mediated knockdown of Xist can rescue the impaired postimplantation development of cloned mouse embryos. *Proc. Natl. Acad. Sci. USA*, **108**, 20621–20626.
19. Okae, H., Hiura, H., Nishida, Y., Funayama, R., Tanaka, S., Chiba, H., Yaegashi, N., Nakayama, K., Sasaki, H. and Arima, T. (2012) Re-investigation and RNA sequencing-based identification of genes with placenta-specific imprinted expression. *Hum. Mol. Genet.*, **21**, 548–558.
20. Wilkinson, L.S., Davies, W. and Isles, A.R. (2007) Genomic imprinting effects on brain development and function. *Nat. Rev. Neurosci.*, **8**, 832–843.
21. Mizuno, Y., Sotomaru, Y., Katsuzawa, Y., Kono, T., Meguro, M., Oshimura, M., Kawai, J., Tomaru, Y., Kiyosawa, H., Nikaido, I. *et al.* (2002) Asb4, Ata3, and Dcn are novel imprinted genes identified by high-throughput screening using RIKEN cDNA microarray. *Biochem. Biophys. Res. Commun.*, **290**, 1499–1505.
22. Smith, R.J., Dean, W., Konfortova, G. and Kelsey, G. (2003) Identification of novel imprinted genes in a genome-wide screen for maternal methylation. *Genome Res.*, **13**, 558–569.
23. Kobayashi, H., Sakurai, T., Imai, M., Takahashi, N., Fukuda, A., Yayoi, O., Sato, S., Nakabayashi, K., Hata, K., Sotomaru, Y. *et al.* (2012) Contribution of intragenic DNA methylation in mouse gametic DNA methylomes to establish oocyte-specific heritable marks. *PLoS Genet.*, **8**, e1002440.
24. da Rocha, S.T., Edwards, C.A., Ito, M., Ogata, T. and Ferguson-Smith, A.C. (2008) Genomic imprinting at the mammalian Dlk1-Dio3 domain. *Trends Genet.*, **24**, 306–316.
25. Tanaka, S., Oda, M., Toyoshima, Y., Wakayama, T., Tanaka, M., Yoshida, N., Hattori, N., Ohgane, J., Yanagimachi, R. and Shiota, K. (2001) Placentomegaly in cloned mouse concepti caused by expansion of the spongiotrophoblast layer. *Biol. Reprod.*, **65**, 1813–1821.
26. Yevtodiyenko, A. and Schmidt, J.V. (2006) Dlk1 expression marks developing endothelium and sites of branching morphogenesis in the mouse embryo and placenta. *Dev. Dyn.*, **235**, 1115–1123.
27. Ogura, A., Inoue, K., Ogonuki, N., Lee, J., Kohda, T. and Ishino, F. (2002) Phenotypic effects of somatic cell cloning in the mouse. *Cloning Stem Cells*, **4**, 397–405.
28. Kawahara, M., Morita, S., Takahashi, N. and Kono, T. (2009) Defining contributions of paternally methylated imprinted genes at the Igf2-H19 and Dlk1-Gtl2 domains to mouse placentation by transcriptomic analysis. *J. Biol. Chem.*, **284**, 17751–17765.
29. Stadtfeld, M., Apostolou, E., Akutsu, H., Fukuda, A., Follett, P., Natesan, S., Kono, T., Shioda, T. and Hochedlinger, K. (2010) Aberrant silencing of imprinted genes on chromosome 12qF1 in mouse induced pluripotent stem cells. *Nature*, **465**, 175–181.
30. Carey, B.W., Markoulaki, S., Hanna, J.H., Faddah, D.A., Buganim, Y., Kim, J., Ganz, K., Steine, E.J., Cassady, J.P., Creyghton, M.P. *et al.* (2011) Reprogramming factor stoichiometry influences the epigenetic state and biological properties of induced pluripotent stem cells. *Cell Stem Cell*, **9**, 588–598.
31. Boiani, M., Eckardt, S., Scholer, H.R. and McLaughlin, K.J. (2002) Oct4 distribution and level in mouse clones: consequences for pluripotency. *Genes Dev.*, **16**, 1209–1219.
32. Cattanach, B.M., Beechey, C.V. and Peters, J. (2004) Interactions between imprinting effects in the mouse. *Genetics*, **168**, 397–413.
33. Itoh, M., Yoshida, Y., Nishida, K., Narimatsu, M., Hibi, M. and Hirano, T. (2000) Role of Gab1 in heart, placenta, and skin development and growth factor- and cytokine-induced extracellular signal-regulated kinase mitogen-activated protein kinase activation. *Mol. Cell. Biol.*, **20**, 3695–3704.
34. Constancia, M., Angiolini, E., Sandovici, I., Smith, P., Smith, R., Kelsey, G., Dean, W., Ferguson-Smith, A., Sibley, C.P., Reik, W. *et al.* (2005) Adaptation of nutrient supply to fetal demand in the mouse involves interaction between the Igf2 gene and placental transporter systems. *Proc. Natl. Acad. Sci. USA*, **102**, 19219–19224.
35. Humpherys, D., Eggan, K., Akutsu, H., Friedman, A., Hochedlinger, K., Yanagimachi, R., Lander, E.S., Golub, T.R. and Jaenisch, R. (2002) Abnormal gene expression in cloned mice derived from embryonic stem cell and cumulus cell nuclei. *Proc. Natl. Acad. Sci. USA*, **99**, 12889–12894.
36. Chiba, H., Hirasawa, R., Kaneda, M., Amakawa, Y., Li, E., Sado, T. and Sasaki, H. (2008) De novo DNA methylation independent establishment of maternal imprint on X chromosome in mouse oocytes. *Genesis*, **46**, 768–774.
37. Wakayama, T., Perry, A.C., Zuccotti, M., Johnson, K.R. and Yanagimachi, R. (1998) Full-term development of mice from enucleated oocytes injected with cumulus cell nuclei. *Nature*, **394**, 369–374.
38. Ogura, A., Inoue, K., Ogonuki, N., Noguchi, A., Takano, K., Nagano, R., Suzuki, O., Lee, J., Ishino, F. and Matsuda, J. (2000) Production of male cloned mice from fresh, cultured, and cryopreserved immature Sertoli cells. *Biol. Reprod.*, **62**, 1579–1584.
39. Mochida, K., Ohkawa, M., Inoue, K., Valdez, D.M. Jr, Kasai, M. and Ogura, A. (2005) Birth of mice after in vitro fertilization using C57BL/6 sperm transported within epididymides at refrigerated temperatures. *Theriogenology*, **64**, 135–143.
40. DePristo, M.A., Banks, E., Poplin, R., Garimella, K.V., Maguire, J.R., Hartl, C., Philippakis, A.A., del Angel, G., Rivas, M.A., Hanna, M. *et al.* (2011) A framework for variation discovery and genotyping using next-generation DNA sequencing data. *Nat. Genet.*, **43**, 491–498.
41. Dodge, J.E., Okano, M., Dick, F., Tsujimoto, N., Chen, T., Wang, S., Ueda, Y., Dyson, N. and Li, E. (2005) Inactivation of Dnmt3b in mouse embryonic fibroblasts results in DNA hypomethylation, chromosomal instability, and spontaneous immortalization. *J. Biol. Chem.*, **280**, 17986–17991.
42. de Vries, W.N., Binns, L.T., Fancher, K.S., Dean, J., Moore, R., Kemler, R. and Knowles, B.B. (2000) Expression of Cre recombinase in mouse oocytes: a means to study maternal effect genes. *Genesis*, **26**, 110–112.
43. Kaneda, M., Hirasawa, R., Chiba, H., Okano, M., Li, E. and Sasaki, H. (2010) Genetic evidence for Dnmt3a-dependent imprinting during oocyte growth obtained by conditional knockout with Zp3-Cre and complete exclusion of Dnmt3b by chimera formation. *Genes Cells*, **15**, 169–179.
44. Hata, K., Okano, M., Lei, H. and Li, E. (2002) Dnmt3l cooperates with the Dnmt3 family of de novo DNA methyltransferases to establish maternal imprints in mice. *Development*, **129**, 1983–1993.
45. Sekita, Y., Wagatsuma, H., Irie, M., Kobayashi, S., Kohda, T., Matsuda, J., Yokoyama, M., Ogura, A., Schuster-Gossler, K., Gossler, A. *et al.* (2006) Aberrant regulation of imprinted gene expression in Gtl2lacZ mice. *Cytogenet. Genome Res.*, **113**, 223–229.

Downloaded from http://hmg.oxfordjournals.org/ at Tohoku University on March 1, 2014

nature chemical biology

ARTICLE

PUBLISHED ONLINE: 15 DECEMBER 2013 | DOI: 10.1038/NCHEMBIO.1410

VMAT2 identified as a regulator of late-stage β-cell differentiation

Daisuke Sakano[1], Nobuaki Shiraki[1], Kazuhide Kikawa[1,2], Taiji Yamazoe[1], Masateru Kataoka[1], Kahoko Umeda[1], Kimi Araki[3], Di Mao[4], Shirou Matsumoto[2], Naomi Nakagata[5], Olov Andersson[6,7], Didier Stainier[6,8], Fumio Endo[2], Kazuhiko Kume[1,10], Motonari Uesugi[4] & Shoen Kume[1,9]*

Cell replacement therapy for diabetes mellitus requires cost-effective generation of high-quality, insulin-producing, pancreatic β cells from pluripotent stem cells. Development of this technique has been hampered by a lack of knowledge of the molecular mechanisms underlying β-cell differentiation. The present study identified reserpine and tetrabenazine (TBZ), both vesicular monoamine transporter 2 (VMAT2) inhibitors, as promoters of late-stage differentiation of *Pdx1*-positive pancreatic progenitor cells into *Neurog3* (referred to henceforth as *Ngn3*)-positive endocrine precursors. VMAT2-controlled monoamines, such as dopamine, histamine and serotonin, negatively regulated β-cell differentiation. Reserpine or TBZ acted additively with dibutyryl adenosine 3′,5′-cyclic AMP, a cell-permeable cAMP analog, to potentiate differentiation of embryonic stem (ES) cells into β cells that exhibited glucose-stimulated insulin secretion. When ES cell–derived β cells were transplanted into AKITA diabetic mice, the cells reversed hyperglycemia. Our protocol provides a basis for the understanding of β-cell differentiation and its application to a cost-effective production of functional β cells for cell therapy.

© 2014 Nature America, Inc. All rights reserved.

Pancreatic cells arise from definitive endoderm and Pdx1-positive (Pdx1+) pancreatic progenitor cells[1], which proliferate and give rise to all three pancreatic lineages: acini, ducts and endocrine islets[2]. Endocrine precursors are characterized by the transient expression of the basic helix-loop-helix transcription factor neurogenin 3 (Ngn3, also known as Neurog3)[2]. Previous studies showed that Ngn3 specifically establishes the endocrine lineages and that loss of Ngn3 precludes endocrine cell development[2,3]. Production of islet cells occurs through the concerted activation of a combination of transcription factors[4]. However, the coordination of cell fate decisions remains poorly understood.

The prevalence of diabetes mellitus in many populations is high, and development of cell replacement therapy through generation of β cells from ES cells is a research priority. Recent studies have shown that mouse or human ES cells can be induced to recapitulate embryonic development of the pancreas[5]. Studies on ES cell differentiation into endodermal or pancreatic cell lineages have shown that stimulation with activin, FGF or retinoic acid, in addition to inhibition of hedgehog signaling by KAAD-cyclopamine, promotes the differentiation into endoderm or pancreatic fates[6,7]. New signal pathways that promote ES cell differentiation into endodermal[8] or pancreatic[9] lineages have been discovered through large-scale screening of cell-permeable, bioactive small molecules. However, it is still difficult to derive mature β cells that secrete insulin in a glucose-dependent manner. A better understanding is needed of the underlying molecular mechanisms that control the late stages of β-cell development, in which Pdx1+ pancreatic progenitor cells develop into Ngn3+ endocrine progenitor cells and insulin-positive (Ins+) β cells and then further differentiate into mature β cells capable of glucose-stimulated insulin secretion (GSIS).

Here, we identified reserpine and TBZ as potent promoters of pancreatic progenitor cell differentiation into functional β cells. This study highlights the use of chemical compound libraries for the identification of new developmental pathways that control progenitor cell differentiation into mature β cells.

RESULTS

Reserpine and TBZ increase Ins+ cells

The present study used large-scale screening of chemical compounds with an ES cell line, SK7, that expresses GFP under the *Pdx1* promoter[10,11]. The *Pdx1*-GFP ES cell line is useful because the expression of *Pdx1* is biphasic (**Fig. 1a**), which enabled the detection of early-stage Pdx1+ pancreatic progenitors and late-stage Pdx1+ Ins+ β cells . We optimized the culture to promote modest basal differentiation with high reproducibility, so that the markers *Sox17*, *Pdx1*, *Ngn3* and *Ins1* were sequentially expressed (**Fig. 1a**).

To screen for compounds that potentiate the differentiation of ES cell–derived Pdx1+ pancreatic progenitor cells into insulin-expressing cells, we tested a library of 1,120 biologically active compounds arrayed as single compounds in DMSO on cultures, starting on day 11 after confirming the appearance of *Pdx1*-GFP+ cells and conducting the assay on day 17 (**Fig. 1a**). Candidate compounds that increased both *Ins1* expression and the number of Ins+ cells relative to vehicle (1% DMSO) were selected as primary hits. The coefficient of variation of this screen was 0.36 ± 0.0447 (± s.d.), which was difficult to minimize further owing to the long assay

[1]Department of Stem Cell Biology, Institute of Molecular Embryology and Genetics, Kumamoto University, Kumamoto, Japan. [2]Department of Pediatrics, Graduate School of Medical Sciences, Kumamoto University, Kumamoto, Japan. [3]Laboratory of Developmental Genetics, Institute of Resource Development and Analysis, Kumamoto University, Kumamoto, Japan. [4]Institute for Chemical Research and Institute for Integrated Cell-Material Sciences, (WPI-iCeMS), Kyoto University, Kyoto, Japan. [5]Division of Reproductive Engineering, Center for Animal Resources and Development, Kumamoto University, Kumamoto, Japan. [6]Department of Cell and Molecular Biology, Karolinska Institute, Stockholm, Sweden. [7]Department of Biochemistry and Biophysics, University of California-San Francisco, San Francisco, California, USA. [8]Department of Developmental Genetics, Max Planck Institute for Heart and Lung Research, Bad Nauheim, Germany. [9]Program for Leading Graduate Schools, Health Life Science Interdisciplinary and Global Oriented (HIGO) Program, Kumamoto University, Kumamoto, Japan. [10]Present address: Department of Neuropharmacology, Graduate School of Pharmaceutical Sciences, Nagoya City University, Nagoya, Japan. *e-mail: skume@kumamoto-u.ac.jp

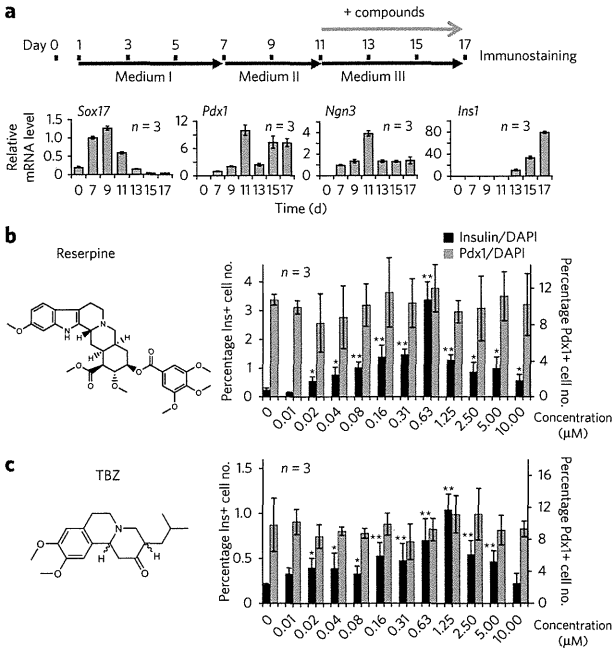

Figure 1 | Reserpine identified as a chemical that enhanced ES cell differentiation into pancreatic β cells. Using a high-throughput screening system, a chemical library was screened, and reserpine was identified as a hit chemical. (**a**) A high-throughput screening system for chemicals that enhance differentiation into β cells. Transcript expressions of *Sox17*, *Pdx1*, *Ngn3* and *Ins1* are expressed as fold change relative to control on day 7. (**b**,**c**) Reserpine (**b**) and TBZ (**c**) (chemical structure shown at left) increased the number of β cells relative to the total number of DAPI-stained cells (black bars) without affecting Pdx1+ cells (light gray bars). In **a**–**c**, data shown are mean ± s.d. ($n = 3$); significant differences between treatment and control at $^*P < 0.05$ and $^{**}P < 0.01$ are shown (two-tailed paired Student's *t*-test).

period. To overcome this, we investigated dose dependencies of the hit chemicals as a secondary screen. Of our hit compounds, the indole alkaloid antipsychotic and antihypertensive drug reserpine demonstrated the strongest effect. Reserpine increased the proportion of Ins+ cells in a concentration-dependent manner without altering the *Pdx1*-GFP+ cell ratio (**Fig. 1b**). Reserpine is known to deplete monoamines from secretory vesicles by blocking uptake into monoamine secretary granules, mediated by VMAT proteins[12–15]. Because human pancreatic β cells express the isoform VMAT2 (refs. 16–19), we also tested another VMAT2 inhibitor, TBZ, which also increased the amount of insulin-expressing cells in a dose-dependent manner (**Fig. 1c**). The half-maximal effective concentration (EC_{50}) values of reserpine and TBZ were 0.19 μM and 0.22 μM, respectively. The concentrations that led to 50% cell death (TD_{50}) were 1.56 μM reserpine and 5.98 μM TBZ. In a separate experiment, we treated cells with 0.63 μM reserpine or 1.25 μM TBZ (**Supplementary Results, Supplementary Fig. 1**). We confirmed the increases in the percentage of Ins+ cells out of the total cell numbers versus the untreated cells and in the relative *Ins1* mRNA levels (by real-time PCR) (**Supplementary Fig. 1**). These results suggested that VMAT2 is the candidate target molecule of reserpine and TBZ, which has a pivotal role in the differentiation of ES cells into Ins-expressing cells.

VMAT2 inhibited differentiation into Ins+ cells

To identify the role of VMAT2 in differentiation of ES cells into pancreatic β cells, we performed a knockdown of VMAT2. We established two VMAT2-knockdown SK7 cell lines, VMAT2KD1 and VMAT2KD2, using lentiviral short hairpin RNA (shRNA) (**Fig. 2a**). VMAT2KD2 exhibited lower *Slc18a2* (henceforth referred to as *Vmat2*) expression than VMAT2KD1 (**Fig. 2a**) and showed greater increases in the number of β cells and level of *Ins1* transcription (**Fig. 2b**). These results indicated that reserpine- or TBZ-mediated VMAT2 inhibition led to an enhancement of differentiation into Ins+ cells. Therefore, VMAT2-mediated monoamine storage functions as a negative regulator of differentiation into Ins+ cells. Pancreatic islets have an isozyme of the monoamine-catabolizing enzyme, monoamine oxidase B (MAO_B)[20]. We then tested the effects of application of pargyline, an MAO_B inhibitor (MAO_{Bi}), to stabilize the monoamines and increase intracellular monoamines. Indeed, application of pargyline had an inhibitory effect on the number of β cells and the level of *Ins1* expression, and reserpine counteracted the inhibitory effect of MAO_{Bi} (**Supplementary Fig. 2**). Moreover, the number and expression level of *Pdx1*-GFP+ cells was unaffected (**Supplementary Fig. 2**), similarly to treatment with reserpine and TBZ (**Fig. 1b,c**).

Monoamines such as dopamine, histamine and serotonin are known to be the substrates for VMAT2. We tested the effect of these monoamines by exogenous application and found that incubation with dopamine, histamine or serotonin from days 11–17 suppressed β-cell differentiation, with EC_{50} values of 1.25 μM (dopamine), 0.5 μM (histamine) and 0.92 μM (serotonin) (**Fig. 2c–e**). We determined the monoamine contents in the ES cell–derived cells on day 17 (**Fig. 2f–h** and **Supplementary Fig. 3a,b**). The dopamine content (approximately 1.3 pg/μg DNA) was approximately 100-fold higher compared to the other monoamines, whereas histamine was undetectable. Inhibition of VMAT2 with TBZ or reserpine and knockdown of *Vmat2* with shRNA significantly decreased ($P < 0.005$) monoamine contents, whereas treatment with pargyline increased it ($P < 0.01$) (**Fig. 2f,h** and **Supplementary Fig. 3**). The enzyme that synthesizes dopamine, tyrosine hydroxylase (Th), was expressed in the ES cells during differentiation at a level comparable to that in the embryonic pancreatic bud. By contrast, the histamine-synthesizing enzyme histidine decarboxylase (Hdc) and the serotonin-synthesizing enzyme tryptophan hydroxylase 1 (Tph1) were expressed at approximately 0.066-fold lower levels compared to those in the embryonic pancreas (**Supplementary Fig. 4a–c**). The monoamine receptors dopamine D2 (Drd2), histamine H1 (Hrh1), histamine H2 (Hrh2) and serotonin 1A (Htr1a) were expressed in day 11 and day 13 differentiated cells (**Supplementary Fig. 4d–f**). Upon addition of chemical compounds that inhibit the synthesizing enzymes for dopamine (α-methyl-tyrosine (α-MT) and L-3,4-dihydroxyphenylalanine (L-DOPA)), histamine (α-fluoromethylhistidine (α-FMH)) or serotonin (5-hydroxy tryptophan (5HTP) and carbidopa), we observed increases in Ins+ cell numbers (**Supplementary Fig. 4g–i**).

Taken together, VMAT2-controlled monoamine release exerted inhibitory effects on the differentiation of pancreatic progenitor cells into Ins+ cells. Reserpine and TBZ inhibit the uptake of monoamines into vesicular stores, which led to depletion of monoamines and potentiation of Ins+ cell differentiation.

TBZ increased differentiation into Ngn3+ cells

We then examined the effects of TBZ on marker expression in ES cell–derived cells by real-time PCR. We used TBZ instead of reserpine owing to its lower cytotoxicity; the results are expressed as fold changes compared to control treatments without chemicals at day 13. Treatment with TBZ resulted in a marked increase of *Ngn3*, *Nkx6-1* and *Ins1* transcripts on day 15 and day 17 (**Fig. 3a**). The real-time PCR results suggested that TBZ increases differentiation of ES cell–derived cells into *Ngn3*+ endocrine progenitors. To follow the transient increase of *Ngn3*+ endocrine precursors in living cells, we developed an NGP9 ES cell line from a transgenic mouse line bearing the *Ngn3*-promoter-driven eGFP transgene[21].

© 2014 Nature America, Inc. All rights reserved.

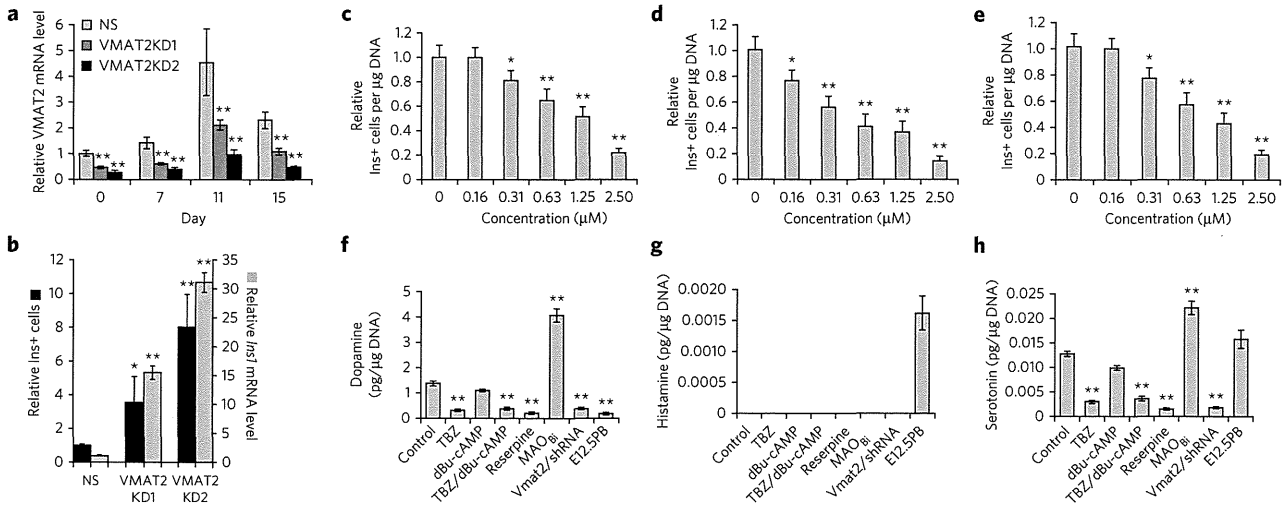

Figure 2 | VMAT2- and monoamine-dependent suppression of pancreatic β-cell differentiation. The effects of VMAT2- and monoamine-mediated inhibition on ES cell differentiation into Ins+ cells were tested, and monoamine cellular contents were determined. (**a**) Time-dependent expression of VMAT2 in VMAT2KD1 (dark gray), VMAT2KD2 (black) and control nonsilencing (NS; light gray) ES cell lines. (**b**) VMAT2KD1 and VMAT2KD2 ES cell lines yielded more Ins+ cells and *Ins1* transcripts than control NS ES cells. (**c**–**e**) Addition of monoamines, dopamine (**c**), histamine (**d**) or serotonin (**e**) suppressed differentiation of ES cells into Ins+ cells in a dose-dependent manner. (**f**–**h**) Cellular contents of dopamine (**f**), histamine (**g**) or serotonin (**h**) when added with VMAT2 inhibitors or MAO_{Bi}, treatment with both TBZ and dBu-cAMP. Control, no chemical treatment; MAO_{Bi}: 1 μM pargyline; Res: 0.63 μM reserpine; MAO_{Bi} + Res: 1 μM pargyline + 0.63 μM reserpine. For **a**–**h**, data shown are mean ± s.d. ($n = 3$); significant differences between treatment and no chemical treatment at $^*P < 0.05$ and $^{**}P < 0.01$ are shown (two-tailed paired Student's *t*-test). In **a** and **b**, black bars indicate Ins+ or *Pdx1*-GFP+ relative cell numbers, and gray bars indicate *Ins1* or *Pdx1* transcript expression relative to that in cells with no chemical treatment.

© 2014 Nature America, Inc. All rights reserved.

We treated the NGP9 cells with TBZ from day 11 to 13 and then performed the assay on day 13 (**Fig. 3b**). TBZ increased *Ngn3*-GFP+ cell numbers (**Fig. 3b**). These results indicate that VMAT2 signaling negatively controls differentiation into *Ngn3*-GFP+ endocrine precursors. We observed 5-ethynyl-2′-deoxyuridine (EdU) incorporation in Ngn3− cells but not in Ngn3+ cells, and TBZ addition did not increase EdU+ Ngn3+ cells, indicating that the increase in Ngn3+ cells was due to increased differentiation into Ngn3+ cells but not proliferation of Ngn3+ cells (**Fig. 3b** and **Supplementary Fig. 5a**). The Ngn3+ cells expressed Nkx2.2 and Nkx6.1 in their nuclei (**Supplementary Fig. 5b**).

We then examined whether this mechanism existed during normal embryonic development using an *in vitro* pancreas bud culture system. Upon addition of TBZ, we observed increased differentiation into insulin-, glucagon-, somatostatin- or pancreas polypeptide–expressing endocrine cells in the *Pdx1*-GFP+

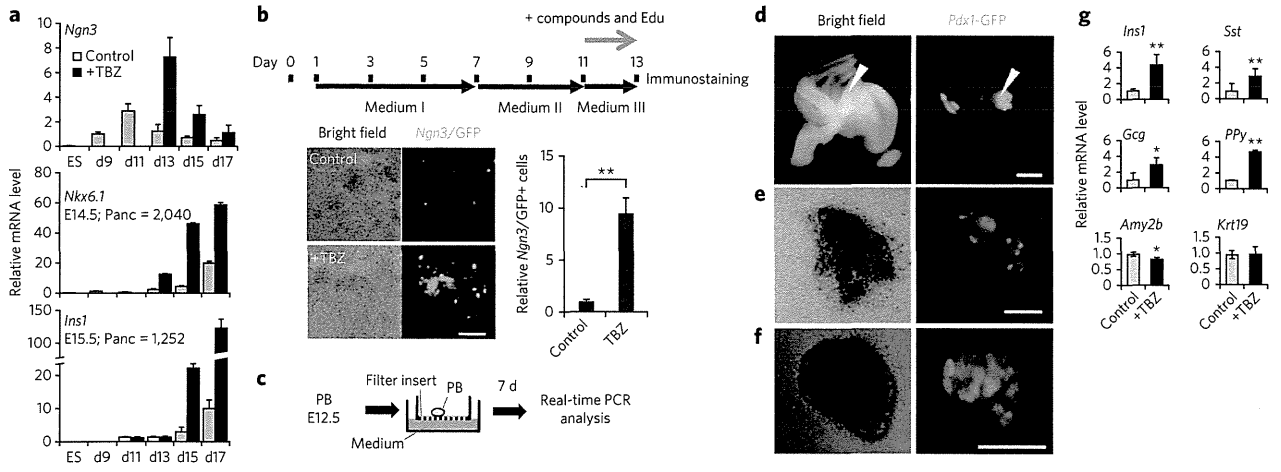

Figure 3 | VMAT2 inhibition increased differentiation into *Ngn3*-GFP+ cells. TBZ increased differentiation into *Ngn3*-GFP+ cells without increasing proliferation. (**a**) *Ngn3*, *Nkx6.1* and *Ins1* expression assayed on differentiation days (d) 13, 15 and 17, with or without (w/o) TBZ, expressed as fold change relative to control on day 13. Gray bars, no chemical (vehicle) samples; black bars, TBZ-treated samples. For all graphs, ($n = 3$). (**b**) A schematic drawing of the experimental design is shown. ES cell cultures were added with TBZ from day 11 to day 13 and assayed on day 13. Transmission or fluorescence images (left) and quantitative representations (right) of *Ngn3*-GFP+ cells without TBZ on day 13 are shown. (**c**) Schematic drawing of the experimental design. Pancreatic rudiments (PB, pancreatic bud) dissected from *Pdx1*-GFP mice at E12.5 were used for *ex vivo* culture for 7 d on filter inserts. (**d**–**f**) Transmission (left) and fluorescence (right) micrographs of explants before (**d**) and after culturing without TBZ (**e**; control DMSO) or with TBZ (**f**). (**g**) Semiquantitative real-time PCR was used to assay the expression of *Gcg*, *Sst*, *PPy*, *Amy2b* or *Krt19* after 7-d culture. Data shown are mean ± s.d. ($n = 3$), expressed as relative cell number compared to control. Scale bars, 200 μm. $^*P < 0.05$ and $^{**}P < 0.01$ (two-tailed paired Student's *t*-test).

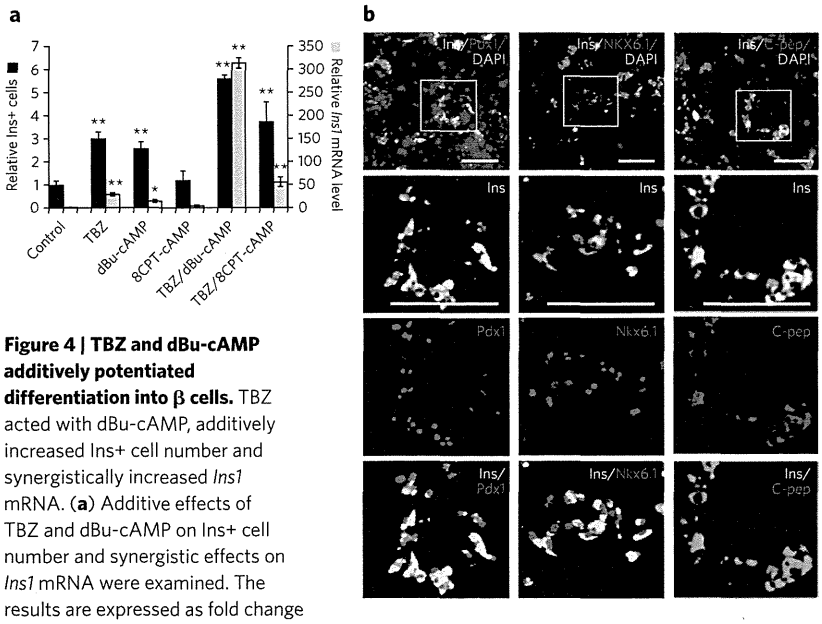

Figure 4 | TBZ and dBu-cAMP additively potentiated differentiation into β cells. TBZ acted with dBu-cAMP, additively increased Ins+ cell number and synergistically increased *Ins1* mRNA. (**a**) Additive effects of TBZ and dBu-cAMP on Ins+ cell number and synergistic effects on *Ins1* mRNA were examined. The results are expressed as fold change relative to control vehicle treatment (DMSO). By contrast, treatment with 8CPT-cAMP, a cAMP analog that specifically activates Epac2, showed no effects. Data shown are mean ± s.d. ($n = 3$), expressed as relative cell number compared to control (no chemical treatment). On the *y* axis, 1 = 0.3% Ins+ cells. (**b**) Total ES cell cultures were assayed by immunohistochemistry. Ins staining (yellow) completely overlapped with staining (red) of Pdx1, Nkx6.1 and C-peptide for *in vitro* differentiated ES cells treated on days 11–17 with TBZ and dBu-cAMP. Blue shows DAPI staining. Scale bars, 100 μm. Lower panels are enlarged pictures of the boxes in the top panels. $^*P < 0.05$ and $^{**}P < 0.01$ (two-tailed paired Student's *t*-test).

pancreatic bud explant culture (**Fig. 3c–g**). We observed a slight decrease in *Amy2b*-expressing exocrine cells but no effects on *Krt19*-expressing duct cells. These results therefore suggested that VMAT2-mediated inhibition of the progress from Pdx1+ pancreatic progenitors to Ngn3+ endocrine progenitors exists in both normal pancreatic endocrine development (**Fig. 3c–g**) and ES cell differentiation (**Fig. 3b**).

The combinatory effects of TBZ and dBu-cAMP addition

Dopamine, histamine and serotonin are considered to function through binding to their receptors. All dopamine, histamine and serotonin receptors are G protein–coupled receptors[22]. In our screen, dibutyryl adenosine 3′,5′-cAMP (dBu-CAMP), a cell-permeable cAMP analog, was identified as a compound to promote β-cell differentiation. We examined the effects of dBu-cAMP and its synergy with TBZ. TBZ or dBu-cAMP alone increased the number of Ins+ cells or the amount of *Ins1* transcript, respectively. Simultaneous addition of TBZ and dBu-cAMP caused an approximately 300-fold increase in *Ins1* transcript, which is approximately 30-fold or 15-fold the effect of single addition of TBZ or dBu-cAMP, respectively (**Fig. 4a**).

In the adult islets, cAMP is known to regulate the potentiation of insulin secretion by a protein kinase A (PKA)-dependent mechanism and a PKA-independent mechanism that involves the cAMP-binding protein Epac2 (ref. 23). As dBu-cAMP activates both pathways[24,25], we then tested a cell-permeable analog, 8CPT-cAMP, that specifically activates Epac2 but not PKA[26]. Ins+ cell number or *Ins1* gene expression did not increase with application of 8CPT-cAMP, and neither showed an additive effect after treatment with 8CPT-cAMP and TBZ. The results suggested that the potentiation of β-cell differentiation by the dBu-cAMP signaling pathway is not mediated through activation of Epac2 but possibly through PKA (**Fig. 4a**).

We then analyzed the differentiated ES cell–derived β cells generated by TBZ and dBu-cAMP treatment by immunocytochemistry. The Ins+ cells expressed Pdx1 and Nkx6.1, which are mature β cell markers. Almost all of the Pdx1+ cells were Ins+. Almost all Ins+ staining overlapped with C-peptide+ staining (**Fig. 4b**). Ins+ cells expressed Nkx2.2, Nkx6.1 and MafA (**Supplementary Fig. 6a**). We also observed *Dolichos biflorus* agglutinin (DBA)+ pancreatic duct cells but not amylase+ exocrine cells in the ES cell culture (**Supplementary Fig. 6b**). There were no qualitative differences in the expression of the above markers among cells treated with both TBZ and dBu-cAMP or each alone (**Supplementary Fig. 6a,b**). We examined whether the Ins+ cells also expressed other endocrine hormones. Although some Ins-single-positive cells, which do not express other endocrine hormones, exist (approximately 10%) in the culture, over 90% of the Ins+ cells were polyhormonal cells, in which glucagon, somatostatin and/or pancreatic polypeptide were also expressed with insulin (**Supplementary Fig. 6**).

As almost all of the Pdx1+ cells derived from ES cells treated with TBZ or dBu-cAMP expressed insulin at the late stage (day 17), which corresponded to the second phase of Pdx1 expression, where Ins is also coexpressed. (**Fig. 1a**), we purified ES cell–derived *Pdx1*-GFP+ cells by flow cytometry (**Fig. 5a,b**) to analyze the β cells with respect to insulin content, GSIS and mRNA expression (**Fig. 5c–e**). *Pdx1*-GFP+ β cells comprised 10.2% of the total cells recovered (**Fig. 5b**). TBZ alone increased C-peptide content to 10 μg per mg, which is approximately 60% of that in adult islets (**Fig. 5c**). However, TBZ did not promote differentiation into cells capable of GSIS (**Fig. 5d**). Isolated *Pdx1*-GFP+ cells treated with dBu-cAMP alone increased GSIS to 170 ng per mg protein per h, which is 42% of that in mature islets (**Fig. 5d**). However, in contrast to TBZ, dBu-cAMP did not increase C-peptide content on a per-protein level (**Fig. 5d**).

The recovery of C-peptide contents from total ES cell–derived cells treated with TBZ, dBu-cAMP or both compounds is summarized in **Supplementary Figure 7a**. ES cell–derived β cells with a C-peptide content equivalent of approximately 100 islets could be obtained from one 96-well plate. The C-peptide contents increased by approximately 5.7-fold or 2.7-fold through treatment with TBZ or dBu-cAMP alone, respectively, and to 8.1-fold through treatment with both compounds (on a per μg DNA basis). This result is consistent with the above result that TBZ and dBu-cAMP additively increased Ins+ cell number.

We also examined the time-dependent effects of the chemicals on GSIS. TBZ alone did not alter GSIS, but dBu-cAMP alone potentiated ES differentiation into Ins+ cells, showing the ability for GSIS from day 15 (**Supplementary Fig. 7b**). To further confirm that the effect of dBu-cAMP occurs through potentiation of differentiation into Ins+ cells, we treated ES cells with dBu-cAMP in different time windows, that is, from day 11 to day 15 or from day 11 to day 17, and then assayed for GSIS on day 17. Treatment with dBu-cAMP for a longer period (day 11 to day 17) significantly ($P < 0.01$) enhanced GSIS compared to those treated from day 11 to day 15 (**Supplementary Fig. 8**). Treatment with dBu-cAMP during the secretion assay significantly ($P < 0.01$) increased GSIS. Therefore, dBu-cAMP treatment potentiated differentiation into matured β cells and enhanced GSIS ability. The results

© 2014 Nature America, Inc. All rights reserved.

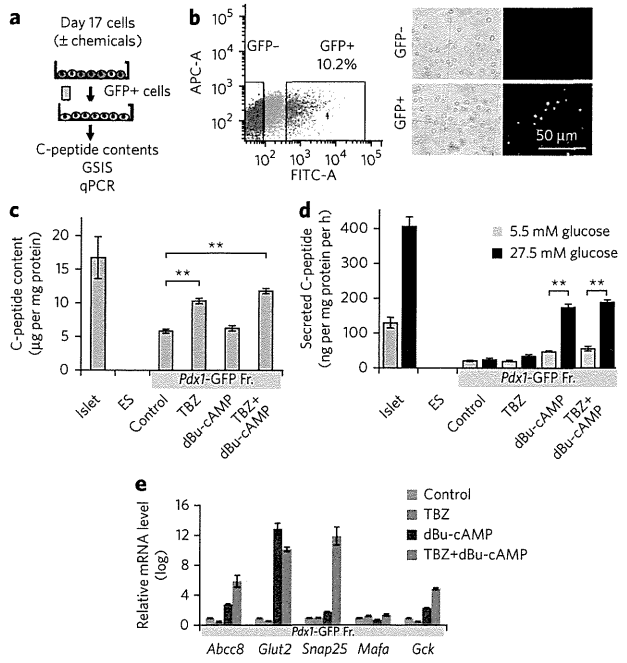

Figure 5 | Characterization of the purified ES cell-derived Ins+ and Pdx-GFP+ cells. TBZ and dBu-cAMP additively potentiated differentiation and maturation of ES cells into β cells with GSIS ability. (**a**–**e**) Differentiated β cells were purified by flow cytometry. Experimental procedures (**a**) and flow cytometry results (**b**) are shown. Cells were tested for their C-peptide contents (**c**), GSIS (**d**) and quantitative PCR (qPCR) (**e**). In **b**, *Pdx1*-GFP+ cells (10.2% of total cells) were purified by flow cytometry on the basis of GFP intensity. Scale bar, 50 μm. In **c** and **d**, treatment with TBZ alone increased C-peptide content, and treatment with dBu-cAMP alone evoked GSIS, as measured by C-peptide contents or secreted C-peptide with significant differences (two-tailed paired Student's *t*-test) $^{**}P < 0.01$. (**e**) Quantitative PCR was performed to quantify the expression of *Abcc8*, *Glut2*, *Snap25*, *Mafa* and *Gck*. In **c**–**e**, GFP+ cells from differentiated ES cells were used, to which DMSO (no chemical treatment), TBZ or dBu-cAMP or both (TBZ + dBu-cAMP) were added. In **c**, $n = 4$, and in **d** and **e**, $n = 3$.

showing that dBu-cAMP potentiated GSIS suggested that the enhancement of differentiation may be mediated by insulin. The effect of insulin was then examined by manipulating the insulin concentration in medium III (**Fig. 1a**), which contained 10 μM insulin in all of the experiments reported so far. Insulin potentiated the differentiation at 16 nM, and its effect declined with increasing insulin concentrations (**Supplementary Fig. 9**). Therefore, TBZ plus dBu-cAMP enhanced insulin secretion at low levels, which in turn accelerated the expression of *Ins1* and further drove β-cell differentiation.

Real-time PCR analyses revealed that dBu-cAMP administration alone increased the expression of genes implicated in GSIS: *Abcc8*, which encodes the regulatory sulfonylurea receptor SUR of the ATP-sensitive potassium channel, and the glucose transporter-encoding genes *Slc2a2* (also known as *Glut2*) and *Gck* (**Fig. 5e**). Double treatment with TBZ and dBu-cAMP upregulated expression of *Abcc8* and *Gck* by ~1×10^5–fold and upregulated expression of *Glut2* and *Snap25*, which encodes a component involved in the regulation of vesicular release, by ~1×10^{10}–fold compared to expression in the control (**Fig. 5e**).

Taken together, these results indicated that TBZ treatment increased insulin content and dBu-cAMP increased GSIS of the ES cell–derived cells. Simultaneous treatment with TBZ and dBu-cAMP enabled the ES cell–derived β cells to produce Ins and secrete Ins *in vitro* in a glucose-sensitive manner at levels comparable to that of adult islets.

The transplanted cells reversed hyperglycemia in mice

To examine their *in vivo* function, we transplanted ES cell–derived β cells into AKITA mice with immunodeficiency (*Rag1*$^{-/-}$ *Ins2*$^{Akita/+}$)[27]. The AKITA mouse is a model that inherits diabetes in a dominant manner owing to a missense mutation in *Ins2*. Consistent with our previous report[28], all male heterogeneous AKITA mice gradually developed hyperglycemia after they reached 6 weeks of age (**Supplementary Fig. 10a**). We harvested 4×10^6 or 1×10^7 ES cell–derived cells (treated with both TBZ and dBu-cAMP) on day 17 and grafted the cells under the kidney capsule in each experimental mouse. The experimental mice showed a reversal of hyperglycemia for more than 6 weeks, with larger grafts showing increasing effects (**Supplementary Fig. 10a**), whereas no change in blood glucose was observed in control untransplanted AKITA mice.

We then transplanted 1×10^7 ES cell–derived cells, which were treated with no chemical, TBZ or dBu-cAMP alone or with both TBZ and dBu-cAMP, into the kidney capsule of the AKITA mice. Mice engrafted with cells that were not treated with growth factors served as negative controls. Mice transplanted with cells treated with TBZ plus dBu-cAMP or dBu-cAMP alone partially recovered from hyperglycemia and showed lowered fasting blood glucose as early as 2 weeks after engraftment (**Fig. 6a**). Mice engrafted with cells treated with both TBZ and dBu-cAMP completely recovered from glucose intolerance, whereas those engrafted with cells treated with dBu-cAMP alone did not (**Fig. 6a–c**). In both cases, the engrafted mice showed even higher levels of plasma C-peptide compared to that in the control wild-type BL6 mice (**Supplementary Fig. 10b**). The AKITA mice are reported to be insulin resistant[29]. The above results might reflect the insulin resistance of the recipient AKITA mice. In contrast, mice engrafted with cells treated with TBZ alone responded to glucose administration and increased plasma C-peptide levels more rapidly compared to those engrafted with control cells (no chemical treatment) (**Supplementary Fig. 10b**), which agreed with their partial reversal of glucose tolerance (**Fig. 6b**) and fasting blood glucose (**Fig. 6a**).

Grafts without noticeable tumor formation were recovered from the experimental mice and were found to express insulin (**Supplementary Fig. 10c**). No insulin-positive cells coexpressed glucagon, pancreas polypeptide or somatostatin. We confirmed that the β-cell mass in the recipient AKITA pancreas did not increase after transplantation, showing an altered allocation of glucagon+ cells at the center of the islets, in contrast to their peripheral localization in the control wild-type mice (**Supplementary Fig. 10d**). Taken together, we concluded that the reversal of hyperglycemia and restoration of glucose tolerance was due to the transplanted ES cell–derived cells.

These results demonstrate that treatment of both TBZ and dBu-cAMP potentiated differentiation of ES cells into cells, with a high level of C-peptide contents and GSIS ability, and transplantation of these cells reversed hyperglycemia in AKITA diabetic mice.

DISCUSSION

Although the function of VMAT2 in the pancreas is largely unknown, VMAT2 is known to take up monoamines such as dopamine, histamine and serotonin into secretory granules of neurons and exert both autocrine and paracrine functions in the nervous system. VMAT2 is described to be expressed in human β cells. However, there has been some controversy in the literature about its presence in β cells of rodents[30]. Here, the target cells of the VMAT2 inhibitors are differentiating pancreatic progenitor cells. We revealed a new role of VMAT2 and monoamine-dependent suppression of differentiation from the pancreatic progenitor cells.

© 2014 Nature America, Inc. All rights reserved.

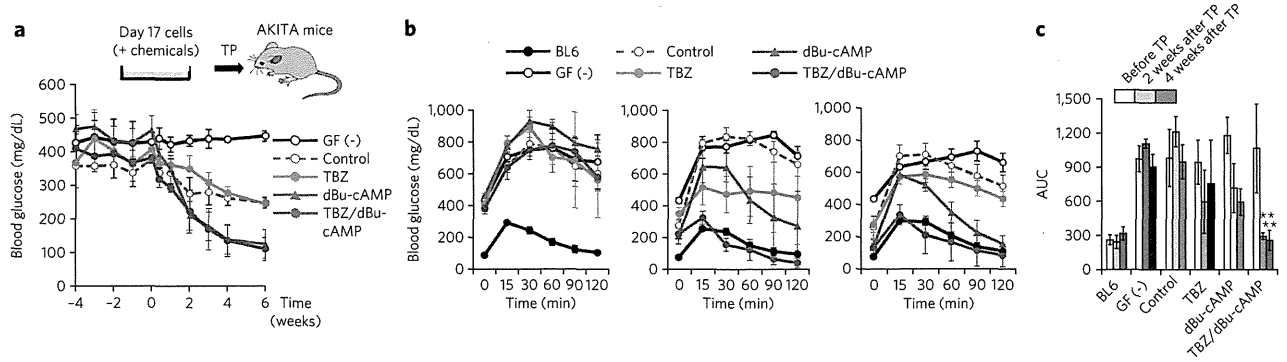

Figure 6 | Transplanted cells reversed hyperglycemia and glucose tolerance. Transplantation assays showed that the induced β cells normalized fasting blood glucose levels and glucose tolerance in the AKITA diabetic mice. (**a**) Top, experimental procedure. *In vitro* differentiated β cells, treated with TBZ and dBu-cAMP, were harvested on day 17 and transplanted into hyperglycemic AKITA mice. Bottom, fasting blood glucose levels (mg/dL) of mice transplanted with ES-derived β cells were measured before and after engraftment. X axis shows weeks after transplantation. (**b**) AKITA mice were analyzed for IPGTT before engraftment (left), 2 weeks (middle) or 4 weeks (right) after engraftment, and time courses of blood glucose levels (mg/dL) after challenge with glucose are shown. X axis shows minutes after glucose challenges. (**c**) Area under curve (AUC) of IPGTT curves shown in **b**. Light color bars, before engraftment; darker color bars, 2 weeks after engraftment; darkest color bars, 4 weeks after engraftment. In **a** and **b**, blue circles represent treatment with TBZ, green circles represent treatment with dBu-cAMP, purple circles represent treatment with TBZ and dBu-cAMP, broken lines with open circles represent no chemical treatment at 1×10^7, and black lines with open circles represent cells with no growth factor treatment (negative controls). In **a**–**c**, *the significant differences between treatment and control were *P < 0.05 or **P < 0.01 (two-tailed unpaired Student's t-test) and are indicated above error* bars, which show s.d.

© 2014 Nature America, Inc. All rights reserved.

Dopamine, histamine and serotonin are synthesized and stored in the endocrine pancreas during pregnancy[31] and in adult β cells[19]. In the adult, there are several lines of evidence supporting that dopamine and histamine negatively regulate insulin content, glucose tolerance[32–34] and GSIS[35–37]. In contrast, serotonin is reported to drive β-cell replication and regulate glucose tolerance in pregnant mice. However, the role of monoamines during embryonic development remains largely unknown.

Among the monoamines, dopamine is produced at a highest level in ES cell–derived cells and during embryonic stages. Consistent with this, dopamine synthesizing enzyme (encoded by *Th*), was expressed in the ES-derived cells at a level comparable to that in the embryonic pancreas. In spite of the differences in their cellular contents, inhibition of all three synthesizing enzymes showed similar effects to enhance β-cell differentiation, indicating that all of these monoamines take part in this process. It was puzzling that application of these monoamines dose-dependently suppressed β cell differentiation with similar EC_{50} values, although their EC_{50} against their specific receptors are very different[38–40]. We hypothesize that this is due to the fact that monoamine is taken up into the storage vesicles and their subsequent release is required for their action and that other components co-released from the vesicle might be required to convey their function[41].

Our results indicated that monoamines controlled by VMAT2 serve as a brake for differentiation of Pdx1+ pancreatic progenitors into Ngn3+ endocrine precursors and subsequently into Ins+ cells. Once this brake is released, the Pdx1+ cells are induced to differentiate into Ngn3+ cells, which quickly turn into Ins+ cells. TBZ acted during a short time window to increase Ngn3+ cells, suggesting that this brake functions transiently. However, whether there are specific roles for each of the monoamines remains an open question.

In the adult β cells, GLP1 and GIP are well known to activate $G\alpha_s$-coupled receptors and potentiate GSIS by activating cAMP signaling and modulating K_{ATP} channel activity. It is reported that cAMP signaling induces glucose responsiveness through both PKA and Epac2 dependent pathway[23]. PKA is reported to modulate VMAT2 by regulating its trafficking[42]. It is possible that cAMP activates β-cell differentiation through modulating VMAT2. It remains unknown whether GLP1, GIP or other unknown ligands function to promote the maturation of β cells to initiate GSIS during embryonic development. This would agree with the observation that pancreas-specific $G\alpha_s$-deficient mice demonstrated reduced β-cell mass and defects in glucose response[43].

Most of the ES cell–derived insulin+ cells were polyhormonal cells, coexpressing other endocrine hormones. Maturation rapidly occurred *in vivo*. They rapidly turned into insulin-single positive cells after they were grafted under kidney capsules. Intrapenitoneal glucose trelant test (IPGTT) results revealed that cells doubly treated with TBZ and dBu-cAMP matured into cells capable of GSIS and restored glucose tolerance as early as 2 weeks after engraftment. Cells treated with TBZ alone or with no chemicals also matured *in vivo* and became potent for GSIS within 2 weeks. In mouse pancreatic development, Ins+ glucagon+ cells appear early in 'first transition', and they do not contribute to the generation of mature β cells[44]. These cells do not express mature endocrine markers[45]. By contrast, Ins+ glucagon+ transitional cells exist transiently during the conversion of α cells into β cells[46,47]. The polyhormonal cells observed in the present study expressed mature endocrine markers. Therefore, the ES cell–derived polyhormonal cells here might have characteristics close to the transitional cells that appear during cell fate conversion rather than those that exist during early mouse embryonic development. Although the exact mechanism of how ES cells mature under *in vivo* environment remains unknown, it is reported that dynamic chromatin remodeling occurs in human ES cells after they are engrafted *in vivo*[48]. Previous studies have shown that human ES cell–derived insulin-expressing cells, which are polyhormonal, differentiate into α cells, instead of β cells, after transplantation[49]. The discrepancies might be due to the differences in the underlying mechanism between the mouse and human ES cells or due to the differences between the culture protocols. However, it is technically difficult for us to perform further long-term analyses, such as transplantation or re-culture of the mouse ES cell–derived Pdx1/GFP+ cells, owing to a significant ($P < 0.01$) loss of cell viability after sorting at this late stage of differentiation. Taken together, although we cannot completely rule out other possibilities, our results suggested that the transplanted insulin-expressing cells reversed hyperglycemia in AKITA mice.

The graft experiments showed that transplanting 4×10^6 or 1×10^7 ES cell–derived cells, with their C-peptide contents equivalent to 40 or 100 islets, respectively, is enough to reverse hyperglycemia in AKITA diabetic mice. This is lower than the previously reported observation that it is necessary to transplant 150–200 islets to reverse hyperglycemia[50]. Our results suggested that these ES cell–derived cells rapidly underwent further differentiation *in vivo* and increased their C-peptide contents or GSIS ability so that a lower number of ES cell–derived cells was enough for the reversal of hyperglycemia.

The ES cell–derived cells showed no signs of tumor formation. This might due to the high differentiation efficiency into the definitive endoderm. Moreover, the long differentiation period might also result in a low population of undifferentiated cells remaining in culture.

In conclusion, results of the present study demonstrated a previously unknown function of VMAT2 in controlling differentiation into pancreatic endocrine precursors. VMAT2 inhibition and dBu-cAMP addition synergized and further increased *Ins1* transcripts and are sufficient to promote differentiation of ES cells into functional β cells capable of reversing hyperglycemia in diabetic mice. Future studies would be required to analyze the role of VMAT2 during human induced pluripotent stem cell cell differentiation to apply this protocol for future cell replacement therapy.

Received 15 December 2012; accepted 15 October 2013; published online 15 December 2013

METHODS

Methods and any associated references are available in the online version of the paper.

References

1. Jonsson, J., Carlsson, L., Edlund, T. & Edlund, H. Insulin-promoter-factor 1 is required for pancreas development in mice. *Nature* **371**, 606–609 (1994).
2. Gu, G., Dubauskaite, J. & Melton, D.A. Direct evidence for the pancreatic lineage: NGN3+ cells are islet progenitors and are distinct from duct progenitors. *Development* **129**, 2447–2457 (2002).
3. Gradwohl, G., Dierich, A., LeMeur, M. & Guillemot, F. *neurogenin3* is required for the development of the four endocrine cell lineages of the pancreas. *Proc. Natl. Acad. Sci. USA* **97**, 1607–1611 (2000).
4. Puri, S. & Hebrok, M. Cellular plasticity within the pancreas—lessons learned from development. *Dev. Cell* **18**, 342–356 (2010).
5. D'Amour, K.A. *et al.* Efficient differentiation of human embryonic stem cells to definitive endoderm. *Nat. Biotechnol.* **23**, 1534–1541 (2005).
6. Skoudy, A. *et al.* Transforming growth factor (TGF)β, fibroblast growth factor (FGF) and retinoid signalling pathways promote pancreatic exocrine gene expression in mouse embryonic stem cells. *Biochem. J.* **379**, 749–756 (2004).
7. D'Amour, K.A. *et al.* Production of pancreatic hormone-expressing endocrine cells from human embryonic stem cells. *Nat. Biotechnol.* **24**, 1392–1401 (2006).
8. Borowiak, M. *et al.* Small molecules efficiently direct endodermal differentiation of mouse and human embryonic stem cells. *Cell Stem Cell* **4**, 348–358 (2009).
9. Chen, S. *et al.* A small molecule that directs differentiation of human ESCs into the pancreatic lineage. *Nat. Chem. Biol.* **5**, 258–265 (2009).
10. Shiraki, N. *et al.* Guided differentiation of embryonic stem cells into Pdx1-expressing regional-specific definitive endoderm. *Stem Cells* **26**, 874–885 (2008).
11. Higuchi, Y. *et al.* Synthesized basement membranes direct the differentiation of mouse embryonic stem cells into pancreatic lineages. *J. Cell Sci.* **123**, 2733–2742 (2010).
12. Wang, Y.M. *et al.* Knockout of the vesicular monoamine transporter 2 gene results in neonatal death and supersensitivity to cocaine and amphetamine. *Neuron* **19**, 1285–1296 (1997).
13. Pothos, E.N. *et al.* Synaptic vesicle transporter expression regulates vesicle phenotype and quantal size. *J. Neurosci.* **20**, 7297–7306 (2000).
14. Vergo, S., Johansen, J.L., Leist, M. & Lotharius, J. Vesicular monoamine transporter 2 regulates the sensitivity of rat dopaminergic neurons to disturbed cytosolic dopamine levels. *Brain Res.* **1185**, 18–32 (2007).
15. Eiden, L.E. & Weihe, E. VMAT2: a dynamic regulator of brain monoaminergic neuronal function interacting with drugs of abuse. *Ann. NY Acad. Sci.* **1216**, 86–98 (2011).
16. Erickson, J.D., Schafer, M.K., Bonner, T.I., Eiden, L.E. & Weihe, E. Distinct pharmacological properties and distribution in neurons and endocrine cells of two isoforms of the human vesicular monoamine transporter. *Proc. Natl. Acad. Sci. USA* **93**, 5166–5171 (1996).
17. Anlauf, M. *et al.* Expression of the two isoforms of the vesicular monoamine transporter (VMAT1 and VMAT2) in the endocrine pancreas and pancreatic endocrine tumors. *J. Histochem. Cytochem.* **51**, 1027–1040 (2003).
18. Simpson, N.R. *et al.* Visualizing pancreatic β-cell mass with [^{11}C]DTBZ. *Nucl. Med. Biol.* **33**, 855–864 (2006).
19. Saisho, Y. *et al.* Relationship between pancreatic vesicular monoamine transporter 2 (VMAT2) and insulin expression in human pancreas. *J. Mol. Histol.* **39**, 543–551 (2008).
20. Grimsby, J., Chen, K., Wang, L.J., Lan, N.C. & Shih, J.C. Human monoamine oxidase A and B genes exhibit identical exon-intron organization. *Proc. Natl. Acad. Sci. USA* **88**, 3637–3641 (1991).
21. Gu, G. *et al.* Global expression analysis of gene regulatory pathways during endocrine pancreatic development. *Development* **131**, 165–179 (2004).
22. Kroeze, W.K., Sheffler, D.J. & Roth, B.L. G-protein-coupled receptors at a glance. *J. Cell Sci.* **116**, 4867–4869 (2003).
23. Seino, S., Shibasaki, T. & Minami, K. Dynamics of insulin secretion and the clinical implications for obesity and diabetes. *J. Clin. Invest.* **121**, 2118–2125 (2011).
24. Lo, K.W., Kan, H.M., Ashe, K.M. & Laurencin, C.T. The small molecule PKA-specific cyclic AMP analogue as an inducer of osteoblast-like cells differentiation and mineralization. *J. Tissue Eng. Regen. Med.* **6**, 40–48 (2012).
25. Mei, F.C. *et al.* Differential signaling of cyclic AMP: opposing effects of exchange protein directly activated by cyclic AMP and cAMP-dependent protein kinase on protein kinase B activation. *J. Biol. Chem.* **277**, 11497–11504 (2002).
26. Kelley, G.G. *et al.* Glucose-dependent potentiation of mouse islet insulin secretion by Epac activator 8-pCPT-2′-*O*-Me-cAMP-AM. *Islets* **1**, 260–265 (2009).
27. Wang, J. *et al.* A mutation in the insulin 2 gene induces diabetes with severe pancreatic β-cell dysfunction in the *Mody* mouse. *J. Clin. Invest.* **103**, 27–37 (1999).
28. Mochida, T. *et al.* Time-dependent changes in the plasma amino acid concentration in diabetes mellitus. *Mol. Genet. Metab.* **103**, 406–409 (2011).
29. Hong, E.G. *et al.* Nonobese, insulin-deficient Ins2Akita mice develop type 2 diabetes phenotypes including insulin resistance and cardiac remodeling. *Am. J. Physiol. Endocrinol. Metab.* **293**, E1687–E1696 (2007).
30. Schäfer, M.K. *et al.* Species-specific vesicular monoamine transporter 2 (VMAT2) expression in mammalian pancreatic β cells: implications for optimising radioligand-based human β cell mass (BCM) imaging in animal models. *Diabetologia* **56**, 1047–1056 (2013).
31. Harris, P.E. *et al.* VMAT2 gene expression and function as it applies to imaging β-cell mass. *J. Mol. Med.* **86**, 5–16 (2008).
32. Fülöp, A.K. *et al.* Hyperleptinemia, visceral adiposity, and decreased glucose tolerance in mice with a targeted disruption of the histidine decarboxylase gene. *Endocrinology* **144**, 4306–4314 (2003).
33. Buchanan, T.A. & Xiang, A.H. Gestational diabetes mellitus. *J. Clin. Invest.* **115**, 485–491 (2005).
34. Kim, H. *et al.* Serotonin regulates pancreatic β cell mass during pregnancy. *Nat. Med.* **16**, 804–808 (2010).
35. Rubí, B. *et al.* Dopamine D2-like receptors are expressed in pancreatic β cells and mediate inhibition of insulin secretion. *J. Biol. Chem.* **280**, 36824–36832 (2005).
36. Ericson, L.E., Hakanson, R. & Lundquist, I. Accumulation of dopamine in mouse pancreatic B-cells following injection of l-DOPA. Localization to secretory granules and inhibition of insulin secretion. *Diabetologia* **13**, 117–124 (1977).
37. Zern, R.T., Bird, J.L. & Feldman, J.M. Effect of increased pancreatic islet norepinephrine, dopamine and serotonin concentration on insulin secretion in the golden hamster. *Diabetologia* **18**, 341–346 (1980).
38. Seeman, P. *et al.* The dopaminergic stabilizer ASP2314/ACR16 selectively interacts with $D2^{High}$ receptors. *Synapse* **63**, 930–934 (2009).
39. Braden, M.R., Parrish, J.C., Naylor, J.C. & Nichols, D.E. Molecular interaction of serotonin 5-HT2A receptor residues $Phe339^{(6.51)}$ and $Phe340^{(6.52)}$ with superpotent *N*-benzyl phenethylamine agonists. *Mol. Pharmacol.* **70**, 1956–1964 (2006).
40. Peakman, M.C. & Hill, S.J. Endogenous expression of histamine H1 receptors functionally coupled to phosphoinositide hydrolysis in C6 glioma cells: regulation by cyclic AMP. *Br. J. Pharmacol.* **113**, 1554–1560 (1994).
41. El Mestikawy, S., Wallen-Mackenzie, A., Fortin, G.M., Descarries, L. & Trudeau, L.E. From glutamate co-release to vesicular synergy: vesicular glutamate transporters. *Nat. Rev. Neurosci.* **12**, 204–216 (2011).
42. Yao, J., Erickson, J.D. & Hersh, L.B. Protein kinase A affects trafficking of the vesicular monoamine transporters in PC12 cells. *Traffic* **5**, 1006–1016 (2004).
43. Xie, T., Chen, M. & Weinstein, L.S. Pancreas-specific Gs_α deficiency has divergent effects on pancreatic α- and β-cell proliferation. *J. Endocrinol.* **206**, 261–269 (2010).

© 2014 Nature America, Inc. All rights reserved.

44. Herrera, P.L. Adult insulin- and glucagon-producing cells differentiate from two independent cell lineages. *Development* **127**, 2317–2322 (2000).
45. Murtaugh, L.C. Pancreas and β-cell development: from the actual to the possible. *Development* **134**, 427–438 (2007).
46. Collombat, P. *et al.* The ectopic expression of Pax4 in the mouse pancreas converts progenitor cells into alpha and subsequently β cells. *Cell* **138**, 449–462 (2009).
47. Thorel, F. *et al.* Conversion of adult pancreatic α-cells to β-cells after extreme β-cell loss. *Nature* **464**, 1149–1154 (2010).
48. Xie, R. *et al.* Dynamic chromatin remodeling mediated by polycomb proteins orchestrates pancreatic differentiation of human embryonic stem cells. *Cell Stem Cell* **12**, 224–237 (2013).
49. Kelly, O.G. *et al.* Cell-surface markers for the isolation of pancreatic cell types derived from human embryonic stem cells. *Nat. Biotechnol.* **29**, 750–756 (2011).
50. Yasunami, Y. *et al.* Vα14 NK T cell-triggered IFN-γ production by Gr-1+CD11b+ cells mediates early graft loss of syngeneic transplanted islets. *J. Exp. Med.* **202**, 913–918 (2005).

Acknowledgments

We thank members of the Gene Technology Center and Center for Animal Resources and Development at Kumamoto University for technical assistance. This work was supported by the Funding Program for Next Generation World-Leading Researchers (to S.K. (no. LS099) and M.U.); the Japan Society for the Promotion of Science, the Realization of Regenerative Medicine (to S.K. and M.U.); the Program for Leading Graduate Schools 'HIGO' (awarded to S.K.); Grants-in-Aid from the Ministry of Education, Culture, Sports, Science and Technology (MEXT), Japan (no. 21390280 to S.K. and no. 22790653 to D. Sakano); and the Collaborative Research Program of Institute for Chemical Research, Kyoto University (grant no. 2010-44). The iCeMS is supported by World Premier International Research Center Initiative, MEXT, Japan.

Author contributions

D. Sakano performed chemical screening, cellular and biochemical analyses; D. Sakano, N.S. and K.U. established the ES cell differentiation system; D. Sakano, K. Kikawa, M.K. and T.Y. performed transplantation assays; K.A. established the ES cell line; S.M., F.E. and N.N. helped maintain AKITA mice; D.M. and M.U. provided and analyzed the chemical library; O.A. and D. Stainier provided chemicals; K. Kume and S.K. provided technical advices, S.K. designed the experiments and wrote the paper. All of the authors discussed the results and commented on the manuscript.

Competing financial interests

The authors declare no competing financial interests.

Additional information

Supplementary information and chemical compound information is available in the online version of the paper. Reprints and permissions information is available online at http://www.nature.com/reprints/index.html. Correspondence and requests for materials should be addressed to S. Kume.

© 2014 Nature America, Inc. All rights reserved.

ONLINE METHODS

Ethics statement. This animal work is approved by the Institutional Review Board for Animal Care and Use of Kumamoto University. All animal procedures were conducted according to Kumamoto University guideline.

ES cell lines. The SK7 ES cell line[10] was established from a transgenic mouse line bearing the *Pdx1*-GFP gene. NGP9 ES cells were established by culturing blastocysts obtained from transgenic mice heterozygous for the *Ngn3*-GFP gene[21]. SK7 and NGP9 cells were maintained on MEF feeder cells in Dulbecco's modified Eagle's medium (DMEM; Invitrogen, Carlsbad, CA) supplemented with leukemia inhibitory factor (LIF), 10% FBS, nonessential amino acids (NEAA), L-glutamine (L-Gln), penicillin and streptomycin (PS) and β-mercaptoethanol (β-ME)[10].

Differentiation of ES cells into pancreatic β cells. For differentiation studies, ES cells were plated at 5,000 cells per well, in Corning 96-well plates with Ultra-Web Synthetic Polyamine Surface (no. 3873XX1, Corning Coster, Cambridge, MS). The cells were cultured for 7 d in Medium I: Dulbecco's Modified Eagle Medium (DMEM: Invitrogen, Glasgow, UK) containing 4,500 mg/L glucose and supplemented with 100 μM nonessential amino acids (NEAA), 2 mM L-glutamine (L-Gln; Nacalai tesque, Japan), 1 mM sodium pyruvate (Invitrogen), 50 units/mL penicillin, 50 μg/mL streptomycin (PS; Nacalai tesque), 100 μM β-mercaptoethanol (β-ME; Sigma-Aldrich), ITS (10 μg/mL insulin (Sigma-Aldrich), 5.5 μg/mL transferrin (Sigma-Aldrich) and 6.7 pg/mL selenium (Sigma-Aldrich)), 0.25% Albmax (Invitrogen), 10 ng/ml recombinant human Activin-A (R&D Systems, Minneapolis, MN) and 5 ng/mL recombinant human bFGF (Peprotech). On days 7–11, the cells were cultured in Medium II: RPMI 1640 medium (Invitrogen) containing 2,000 mg/L glucose (Sigma, St. Louis, MO), 1 μM retinoic acid (Sigma-Aldrich), 50 ng/mL human recombinant fibroblast growth factor-10 (human recombinant FGF10, Peprotech, Rocky Hill, NJ), 2% B-27 Supplement (Invitrogen) and 0.25 μM of the Shh signaling antagonist 3-keto-*N*-(aminoethyl-aminocaproyl-dihydrocinnamoyl) cyclopamine (KAAD-cyclopamin, Calbiochem, San Diego, CA). Finally, on days 11–17, cells were cultured in Medium III: DMEM containing 1,000 mg/L glucose supplemented with NEAA, L-Gln, PS, β-ME, ITS, 0.25% Albmax (Invitrogen), 10 nM glucagon-like peptide 1 (GLP-1, Sigma-Aldrich) and 10 mM nicotinamide (NA, Sigma-Aldrich). The medium was replaced every 2 d.

Screening of small molecules and quantitative analysis of imaging. Small molecules from the bioactive, pharmacologically defined Prestwick Chemical Library were screened for pro-differentiation factors. Compounds were dissolved in DMSO (Sigma-Aldrich) and added at 1:100 on day 11, with changes on days 13 and 15. Cells were assayed by immunostaining with mouse anti-insulin (Sigma-Aldrich; I2018; 1:1,000) on day 17. Fluorescent images were quantified by counting pixel numbers representing the number of positive cells, using a ImageXpress Micro scanning system and MetaXpress cellular image analysis software (Molecular Devices, Japan). Data were normalized as fold change relative to DMSO controls. Hit compounds were defined as causing a twofold or higher increase in insulin-positive β cells. Candidate compounds were tested for dose dependency and reproducibility. The screening information is summarized in **Supplementary Table 1**.

Chemicals. Reserpine was purchased from Calbiochem Novabiochem Novagen, TBZ was purchased from Tocris Bioscience, and dibutyryl-cAMP (dBu-cAMP) was purchased from BIOMOL International.

Pargyline was purchased from Cayman Chemicals. The compounds were dissolved in DMSO (final concentration = 1.0%) and added on days 11, 13 and 15. After initial screening, the following concentrations were used: 0.63 μM reserpine, 1.25 μM TBZ, 0.1 μM dopamine (LKT Labs, Inc.), 0.6 μM dBu-cAMP, 1.0 μM pargyline, 1.3 μM α-methyltyrosine (α-MT, Sigma-Aldrich), 0.6 μM L-3,4-dihydroxyphenylalanine (L-DOPA, Toronto Research Chemicals Inc,), 1.3 μM α-fluoromethyl- histidine (α-FMH, Toronto Research Chemicals Inc,), 1.3 μM 5-hydroxy tryptophan (5HTP, Sigma-Aldrich) and 0.6 μM carbachol (Sigma-Aldrich), unless otherwise specified.

Chemical characterization. To confirm the purity of reserpine, TBZ and dBu-cAMP, we checked their HPLC, LC-MS (ESI), and ^{1}H-NMR profiles. The results showed that the reagents we used had high purity (>90%) (**Supplementary Figs. 11–13**). HPLC analysis was performed with a Shimadzu LC-2010C equipped with reversed-phase HPLC column (GL science, Inertsil ODS-3, 4.6 × 150 mm, flow rate 1.0 mL/min, 0.1% TFA CH_3CN/H2O, 10–100%). Mass spectra (ESI) were recorded on a Shimadzu LCMS-2010. ^{1}H-NMR spectra were collected on a JEOL JNM-ECP (300 MHz).

Immunocytochemistry. For immunocytochemistry, ES cells were fixed with 4% paraformaldehyde and processed after 13 days in culture (**Fig. 3** and **Supplementary Fig. 5**), 17 d in culture (**Figs. 1, 2** and **4** and **Supplementary Fig. 6**) or 6 weeks after transplantation (**Supplementary Fig. 10**). For examination of target protein expression in single cells, ES cell–derived differentiated cells were dissociated with 0.25% trypsin (Invitrogen), replated for 30 min and then fixed and processed for immunocytochemistry. The following antibodies were used: rabbit anti-MafA (Abcam; ab17976; 1/100,), rabbit anti–C-peptide (Cell Signaling; 4593, 1/100), guinea pig anti-insulin (Dako; A0564; 1/1,000), rabbit anti-pancreatic polypeptide (Dako; A619; 1/100), mouse anti-Nkx2.2 (Developmental Studies Hybridoma Bank, University of Iowa; 74.5A5; 1/100), mouse anti-Nkx6.1 (Developmental Studies Hybridoma Bank, University of Iowa; F64A6B4; 1/100), rabbit anti-GFP (MBL International Corp; 598; 1/1,000), goat anti-Pdx1 (R&D systems; AF2419, 1/100), goat anti-amylase (Santa Cruz Biotechnology; sc-12821; 1/100), goat anti-somatostatin (Santa Cruz Biotechnology; sc-7819; 1/100), mouse anti-glucagon (Sigma-Aldrich; G2654; 1/1,000), biotin-conjugated *D. biflorus* agglutinin (DBA) lectin (Sigma-Aldrich; L6533; 1/500) and mouse anti-insulin (Sigma-Aldrich; I2018; 1/1,000) antibodies were used. Secondary antibodies used were Alexa 488–conjugated goat anti-mouse IgG (A11029; 1/1,000), Alexa 568–conjugated goat anti-guinea pig IgG (A11075; 1/1,000), Alexa 568–conjugated goat anti-mouse IgG (A11031; 1/1,000), Alexa 568–conjugated goat anti-rabbit IgG (A11036; 1/1,000), Alexa 568–conjugated anti-streptabidine antibody (S11223; 1/1,000), or Alexa 633–conjugated donkey anti-goat IgG (A21082; 1/1,000), Alexa 633–conjugated goat anti-mouse IgG (A21053; 1/1,000), Alexa 633–conjugated goat anti-rabbit IgG (A21072; 1/1,000) (all from Invitrogen). Cells were counterstained with DAPI (Roche Diagnotics, Basel, Switzerland).

Gene silencing. In the VMAT2-knockdown assays, cells were transfected with Expression Arrest nonsilencing, control shRNA (Open Biosystems, no. RHS4080), VMAT2 shRNA (Open Biosystems, no. RMM3981-97058457 and no. RMM3981-97058458). The lentiviral vectors were constructed as previously described[11]. SK7 cells were infected with viral supernatants. After 24 h of incubation, the virus-containing medium was replaced with fresh ES maintenance medium. After 24 h of incubation, infected cells were selected using 1.5 μg/mL puromycin (Sigma-Aldrich). The surviving cells were harvested, and clones were selected to establish knockdown and control cell lines.

Measurement of intracellular monoamine levels. Cells were treated with chemicals before harvest (days 11–17). Cells were lysed with lysis buffer containing 0.1% Triton X-100 (Nakarai Tesque, Japan) in 0.1 M PBS (pH7.2, Sigma-Aldrich) with protease inhibitor cocktail. Lysates were assayed for dopamine, histamine, serotonin, adrenaline or noradrenaline with each monoamine-specific ELISA kit (Labor Diagnostika Nord GmbH & Co.; KG Nordhorn Germany).

EdU incorporation. Cells were treated with culture medium containing 20 μM 5-ethynyl-2′-deoxyuridine (EdU) for 48 h before harvest (days 17–19), processed using the Click-iT EdU Alexa Fluor 594 Imaging Kit (Invitrogen) and stained with DAPI and anti-GFP antibodies, rabbit anti-GFP (no. 598; 1:1,000; MBL International Corp., Woburn, MA) and detected with Alexa 488-conjugated goat anti-rabbit IgG (Invitrogen; A-11008; 1:1,000).

Pancreas bud *in vitro* culture. Pancreas buds were dissected from E12.5 embryos of a transgenic mouse line bearing the *Pdx1*- green fluorescent protein (GFP) gene. The tissue was placed onto 12-well Corning Transwell cell culture inserts (Corning Coster, Cambridge, MS). The bottom of the inserts were touched with medium containing M199 with NEAA, L-Gln, PS, β-ME and 10% FBS (FBS, Hyclone).

Flow cytometry. Cells were collected and suspended in 1 × HANKS with 1% FBS. A FACS Aria II flow cytometry cell sorter (Becton Dickinson Immunocytometry Systems, San Jose, CA) was used to purify GFP-positive cells by sorting them against the fluorescence profiles of differentiating cells prepared from wild-type mice. Dead cells were identified using propidium iodide (Sigma-Aldrich).

© 2014 Nature America, Inc. All rights reserved.

Quantitative real-time PCR. RNA was extracted from ES cells, mouse tissue or transplanted grafts using the RNeasy minikit (Qiagen, Hilden, Germany) and then treated with DNase I (Qiagen).

Complementary DNA was synthesized from 1 μg of total RNA using Revertra Ace qPCR RT Master Mix (Toyobo).

For real-time PCR analysis, the mRNA expression was quantified with SyberGreen on an ABI 7500 thermal cycler (Applied Biosystems, Foster City, CA). The level of expression of each gene was normalized with that of the β-actin–expressing gene *Actb*. The PCR conditions were as follows: denaturation at 95 °C for 15 s, annealing and extension at 60 °C for 60 s for up to 40 cycles. Each measurement was normalized to *Actb* (mouse) expression for each sample by subtracting the average *Actb* (mouse) expression. C_t values (threshold cycle) from the average Each gene C_t, resulting in C_t Target mRNA levels are expressed as arbitrary units. All of the primers for real-time PCR are listed in **Supplementary Table 2**.

Measurement of glucose-stimulated C-peptide secretion and cellular or plasma C-peptide level by enzyme-linked immunosorbent assay. Differentiating ES cells were preincubated for 0.5 h in low glucose (5.5 mM) DMEM with minimal essential medium and 1% FBS. Cells were washed twice with phosphate-buffered saline then incubated for 2 h in low-glucose (5.5 mM) or high-glucose (27.5 mM) DMEM with 1% FBS. The culture medium was collected, and cells were lysed with a lysis buffer of 0.1% Triton X-100 in PBS with added protease inhibitor cocktail. Insulin secretion into the culture medium and insulin content of the cell lysates were measured using a mouse C-peptide ELISA kit (Shibayagi Co. Ltd., Japan).

IPGTT. Mice fasted for 16–18 h were used. Body weights were measured. Blood glucose levels were measured before (0 min) or at 15 min, 30 min, 60 min, 90 min and 120 min after intraperitoneal administration of 25% Glucose (Sigma-Aldrich) solution at 2 g per kg body weight. Serum C-peptide concentrations were measured as described above.

Cell transplantation into AKITA mice. Differentiated cells were dissociated with 0.25% trypsin, resuspended in DMEM with 10% FBS and injected under the kidney capsules of AKITA mice (C57BL/6J-*Rag1*$^{-/-}$*Ins2*$^{Akita/+}$; male)[27] with a 24G catheter (NIPRO, Japan). The AKITA mice were at least 6 weeks old. Six weeks after transplantation, the tissue was removed and analyzed for insulin expression, content and secretion, as described above.

Statistical tests. Data were analyzed by two-tailed *t*-test. Data are presented as mean ± s.d.

© 2014 Nature America, Inc. All rights reserved.

doi:10.1038/nchembio.1410

Biochimica et Biophysica Acta 1840 (2014) 1355–1359

Contents lists available at ScienceDirect

Biochimica et Biophysica Acta

journal homepage: www.elsevier.com/locate/bbagen

Diagnosis and molecular basis of mitochondrial respiratory chain disorders: Exome sequencing for disease gene identification☆,☆☆

A. Ohtake [a,*], K. Murayama [b], M. Mori [c], H. Harashima [a], T. Yamazaki [a], S. Tamaru [d], Y. Yamashita [d], Y. Kishita [d], Y. Nakachi [d], M. Kohda [d], Y. Tokuzawa [d], Y. Mizuno [d], Y. Moriyama [d], H. Kato [d], Y. Okazaki [d]

[a] Department of Pediatrics, Faculty of Medicine, Saitama Medical University, Saitama 350-0495, Japan
[b] Department of Metabolism, Chiba Children's Hospital, Chiba 266-0007, Japan
[c] Department of Pediatrics, Jichi Medical University, Tochigi 329-0498, Japan
[d] Research Center for Genomic Medicine, Saitama Medical University, Saitama 350-0495, Japan

ARTICLE INFO

Article history:
Received 30 September 2013
Received in revised form 13 January 2014
Accepted 14 January 2014
Available online 24 January 2014

Keywords:
Mitochondrial respiratory chain disorder
Blue native polyacrylamide gel
Electrophoresis
Exome sequencing
Narrowing down protocol

ABSTRACT

Mitochondrial disorders have the highest incidence among congenital metabolic diseases, and are thought to occur at a rate of 1 in 5000 births. About 25% of the diseases diagnosed as mitochondrial disorders in the field of pediatrics have mitochondrial DNA abnormalities, while the rest occur due to defects in genes encoded in the nucleus. The most important function of the mitochondria is biosynthesis of ATP. Mitochondrial disorders are nearly synonymous with mitochondrial respiratory chain disorder, as respiratory chain complexes serve a central role in ATP biosynthesis. By next-generation sequencing of the exome, we analyzed 104 patients with mitochondrial respiratory chain disorders. The results of analysis to date were 18 patients with novel variants in genes previously reported to be disease-causing, and 27 patients with mutations in genes suggested to be associated in some way with mitochondria, and it is likely that they are new disease-causing genes in mitochondrial disorders. This article is part of a Special Issue entitled Frontiers of Mitochondrial Research.

© 2014 The Authors. Published by Elsevier B.V. All rights reserved.

1. Introduction

1.1. Mitochondrial disorders

Mitochondrial disorders have the highest incidence among congenital metabolic disorders, and are thought to occur at a rate of 1 in 5000 births [1]. The common view of mitochondrial disorders is that they include mitochondrial encephalopathy and myopathy, with onset due to mitochondrial DNA defects inherited through the maternal line. In fact, however, only about 25% of the diseases diagnosed as mitochondrial disorders in the field of pediatrics have mitochondrial DNA abnormalities [2,3], while the rest occur due to defects in genes encoded in the nucleus. Most cases are sporadic (do not have a clear genetic association), and a majority of cases resulting from nuclear gene abnormalities are autosomal recessive. Mitochondrial DNA has a circular structure with a length of 16.6 kbp, and encodes only 13 proteins [4]. These 13 proteins are part of the structural composition of complex I (7 proteins), complex III (1 protein), complex IV (3 proteins) and complex V (2 proteins) in the respiratory chain. They do not include any complex II structural proteins. The remaining genes encoded in mitochondrial DNA are 22 tRNAs and two ribosomal RNAs, and mitochondrial disorders due to defects in these RNAs have also been reported. Meanwhile, a certain amount of the gene products encoded in the nucleus exists in the mitochondria, and roughly 1500 are thought to serve important roles in mitochondrial function [5]. In this analysis, we focused on mitochondrial disorders thought to occur due to defects in genes encoded in the nucleus. Mitochondria have many functions, one of the most important being biosynthesis of energy (ATP), and we assume for the following discussion that mitochondrial disorders are nearly synonymous with mitochondrial respiratory chain disorders (MRCD), as respiratory chain complexes [6] serve a central role in ATP biosynthesis.

1.2. Mitochondrial disorders of nuclear origin

As stated above, of the approximately 1500 genes encoded in the nucleus that are thought to be involved in biosynthesis and mitochondrial function, more than 100 have been reported to be causes of mitochondrial disorders [7–9] (Table 1). Among these, about 90% of genes have an autosomal recessive inheritance pattern, and only a small portion

Abbreviations: MRCD, mitochondrial respiratory chain disorder; BN-PAGE, blue native polyacrylamide gel electrophoresis; iPS, induced pluripotent stem cells; LIMD, lethal infantile mitochondrial disease; LCSH, Long Contiguous Stretch of Homozygosity

☆ This is an open-access article distributed under the terms of the Creative Commons Attribution-NonCommercial-No Derivative Works License, which permits non-commercial use, distribution, and reproduction in any medium, provided the original author and source are credited.

☆☆ This article is part of a Special Issue entitled Frontiers of Mitochondrial Research.

* Corresponding author. Fax: +81 49 276 1790.
E-mail address: akira_oh@saitama-med.ac.jp (A. Ohtake).

0304-4165/$ – see front matter © 2014 The Authors. Published by Elsevier B.V. All rights reserved.
http://dx.doi.org/10.1016/j.bbagen.2014.01.025

Table 1
The genetic basis of MRCD.

mtDNA mutations: 35/37 genes	
tRNAs, subunits, rRNAs, and deletions & duplications	
Nuclear mutations: 117 genes	
Nuclear-encoded subunits: 27/~80 genes	**mtDNA replication: 5 genes**
Complex I: *NDUFV1, 2, NDUFB3, 9 NDUFA1, 2, 9, 10, 11, 12, NDUFS1, 2, 3, 4, 6, 7, 8*	*POLG, POLG2, C10orf2, MPV17, AGK*
Complex II: *SDHA, SDHB, SDHC, SDHD*	**mtDNA expression: 24 genes**
Complex III: *UQCRB, UQCRQ*	*LRPPRC, TACO1, MTPAP, MRPS16, MRPS22,MRPL3, GFM1,TSFM,TUFM,TRMU,C12orf65,MTFMT, DARS2, RARS2,YARS2,SARS2,AARS2,HARS2,MARS2,EARS2, RMND1, MTO1, FARS2, GFM2*
Complex IV: *COX6B1, COX4I2, COX7B*	
Complex V: *ATP5E*	
Import, processing, assembly: 38 genes	**Nucleotide transport, synthesis: 9 genes**
Complex I: *C8orf38, C20orf7, NDUFAF1, F2, F3, F4, FOXRED1, NUBPL, ACAD9, AIFM1*	*SLC25A4, SLC25A3, TYMP, DGUOK, TK2, PUS1, SUCLA2, SUCLG1, RRM2B*
Complex II: *SDHAF1, SDHAF2*	**Membrane composition: 14 genes**
Complex III: *BCS1L, HCCS, TTC19*	*COQ2, COQ6, COQ9, PDSS1, PDSS2, CABC1, SERAC1, MPC1, NMT, TAZ, CYCS, OPA1, MFN2, DNM1L*
Complex IV: *SURF1, SCO2, SCO1, COX10, COX15, ETHE1, FASTKD2, C2orf64, C12orf62*	
Complex V: *ATPAF2, TMEM70*	
Multiple: *TIMM8A, SPG7, HSPD1, AFG3L2, DNAJC19, GFER*	
Iron/FeS: *FXN, ISCU, GLRX5, ABCB7, NFU1, BOLA3*	
117 nuclear gene defects	Categories are based on D.R Thorburn's paper[7]

95: autosomal recessive.
10: autosomal dominant.
5: recessive or dominant.
7: X-linked.

have a dominant inheritance pattern [10]. There have also been seven reported cases of mitochondrial disorders from defects in genes encoded by the X chromosome. By function, these include genes involved in the structural composition of the complexes and mitochondrial biosynthesis, genes involved in membrane composition, genes involved in the synthesis and transport of nucleic acids, genes involved in regulating the expression of mitochondrial DNA, and genes involved in mitochondrial DNA replication.

We have actively analyzed the exomes of patients with MRCD in order to identify the cause. Here, we briefly describe our project and discuss the results of exome analyses performed to date, touching on some of the problems that have been encountered.

2. Outline of exome analysis project for MRCD patients

Fig. 1 outlines our current project. It is supported by the Ministry of Education, Culture, Sports, Science and Technology's Research Program of Innovative Cell Biology by Innovative Technology (Cell Innovation) (http://www.cell-innovation.org/english/html/program/theme_010_okazaki.html). First, analyses of enzyme activity [11], quantity and size were performed using fibroblasts from patient skin or biopsy specimens from diseased organs of patients suspected of having MRCD in clinical practice [12]. Quantity and size were analyzed using blue native polyacrylamide gel electrophoresis (BN-PAGE) [13]. Next, among patients in whom decreased enzyme activity or complex formation abnormalities were seen biochemically, whole exome analysis was performed in those with no known mitochondrial DNA abnormalities, and the obtained candidate causal genes were confirmed at the cellular level by rescue experiment or other methods, such as siRNA experiment. Many patients with mitochondrial disorders have primary symptoms in the central nervous system, but brain biopsy in these patients is untenable. Therefore, induced pluripotent stem (iPS) cells were created using fibroblasts from the skin of patients from whom informed consent was obtained. These iPS cells were then differentiated into neurons and glia cells to reproduce the pathology of mitochondrial dysfunction that occurs specifically in the nervous system, based on the notion that this may lead to treatment at the cellular level and ultimately to treatment in humans.

3. Clinical diagnosis of MRCD

Mitochondria exist in all tissues, and symptoms are presented in various organs and/or pathological entities. In pediatric MRCD, symptoms are broadly divided into: (1) encephalomyopathy symptoms; (2) gastrointestinal/hepatic symptoms; and (3) myocardial symptoms [14]. So-called "mitochondrial encephalomyopathy," which has traditionally been considered the main form of mitochondrial disease, belongs among the relatively mild mitochondrial diseases and occurs mostly in older people. Fig. 2 shows a breakdown of clinical diagnoses of mitochondrial disorders in our institute as of January 2013 [15]. Patients with the traditionally described nerve and muscle symptoms numbered 111 in total, including 50 with Leigh syndrome, 11 with neurodegenerative disorders for which no clear cause could be identified, and 50 with so-called "mitochondrial encephalomyopathy." These 111 patients accounted for 40% of the total of 275 patients. Conversely, other forms accounted for two-thirds of cases, among which were 49 cases of lethal infantile mitochondrial disease (LIMD). Together with non-lethal infantile mitochondrial disease (NLIMD), which follows the same course but in which patients survive beyond 1 year of age, the number reached 71, and was by far the most common clinical diagnosis. LIMD encompasses hyperlactacidemia occurring in the neonatal period together with multiple organ failure. Most cases have poor outcomes, and it is thought that most of these patients died with the cause remaining unknown and no diagnosis established. Next were mitochondrial disorders showing single organ dysfunction only, such as mitochondrial hepatopathy (12%) and cardiomyopathy (7%).

4. Exome analysis of MRCD patients

As most mitochondrial diseases occur sporadically with only a few cases discovered in one family line, linkage analysis using a large pedigree cannot be applied, thus suggesting that we cannot use information on chromosomal localization for causal gene identification. When identifying disease-causing genes using bioinformatics analysis for exome data, knowledge of the inheritance patterns is very important [16]. As approximately 90% of MRCD-causing genes show a recessive mode of